

Electron Accepting Units of the Diheme Cytochrome *c* TsdA, a Bifunctional Thiosulfate Dehydrogenase/Tetrathionate Reductase*

Julia M. Kurth^{‡1,2}, José A. Brito^{§1,3}, Jula Reuter^{‡4}, Alexander Flegler[‡], Tobias Koch[‡], Thomas Franke[‡], Eva-Maria Klein^{‡5}, Sam F. Rowe^Σ, Julea N. Butt^Σ, Kevin Denkmann^{‡6}, Inês A.C. Pereira[§], Margarida Archer^{§7}, Christiane Dahl^{‡8}

From the [‡]Institut für Mikrobiologie & Biotechnologie, Rheinische Friedrich-Wilhelms-Universität Bonn, 53115 Bonn, Germany, [§]Instituto de Tecnologia Química e Biológica António Xavier, Universidade Nova de Lisboa (ITQB-UNL), Oeiras, Portugal, ^ΣCentre for Molecular and Structural Biochemistry, School of Chemistry, and School of Biological Sciences, University of East Anglia, Norwich Research Park, Norwich NR4 7TJ, United Kingdom

Running title: *Electron accepting units of TsdA*

Keywords: Cytochrome *c*, enzyme kinetics, protein chemistry, respiratory chain, TsdA, electron acceptor, crystal structure, thiosulfate dehydrogenase

* This work was supported by the Deutsche Forschungsgemeinschaft Grant Da 351/7-2 and Fundação para a Ciência e Tecnologia through iNOVA4Health Research Unit (LISBOA-01-0145-FEDER-007344) cofunded by FCT/MCES and FEDER under the PT2020 Partnership Agreement, through R&D unit, UID/Multi/04551/2013 (GreenIT) and MostMicro unit financially supported by: Project LISBOA-01-0145-FEDER-007660 (Microbiologia Molecular, Estrutural e Celular) funded by FEDER funds through COMPETE2020 - Programa Operacional Competitividade e Internacionalização (POCI) and by national funds through FCT. SFR was supported by a studentship from the UK Biotechnology and Biological Sciences Research Council (BBSRC) and JNB by a Royal Society Leverhulme Trust Senior Research Fellowship.

The atomic coordinates and structure factors (entry 5LO9) have been deposited in the Protein Data Bank (<http://www.pdb.org/>)

¹ Both authors contributed equally to this work

² Recipient of scholarship 700051 funded by the Aventis Foundation and awarded by the Fonds der Chemischen Industrie

³ Recipient of FCT Fellowship SFRH/BPD/79224/2011

⁴ Current affiliation: Rheinische Friedrich-Wilhelms-Universität Bonn, Institut für Pharmazeutische Mikrobiologie, Meckenheimer Allee 168, 53115 Bonn, Germany

⁵ Current affiliation: Rheinische Friedrich-Wilhelms-Universität Bonn, Institut für Virologie, Siegmund-Freud-Str. 25, 53127 Bonn, Germany

⁶ Current affiliation: Dunn Labortechnik GmbH, Thelenberg 6, 53567 Asbach, Germany

⁷ Awarded FCT Investigator IF/00656/2014. To whom correspondence should be addressed: Tel. 351-214-469-747; Fax 351-214-433-644; E-mail: archer@itqb.unl.pt.

⁸ To whom correspondence should be addressed: Tel. 49-228-732119; Fax 49-228-737576; E-mail ChDahl@uni-bonn.de.

ABSTRACT

The enzymes of the thiosulfate dehydrogenase (TsdA) family are wide-spread diheme *c*-type cytochromes. Here, redox carriers were studied mediating the flow of electrons arising from thiosulfate oxidation into respiratory or photosynthetic electron chains. In a number of organisms, including *Thiomonas intermedia* and *Sideroxydans lithotrophicus* the *tsdA* gene is immediately preceded by *tsdB* encoding for another diheme cytochrome. Spectrophotometric experiments in combination with enzymatic assays in solution showed that TsdB acts as an effective electron acceptor of TsdA *in vitro* when TsdA and TsdB originate from the same source organism. While TsdA covers a range from -300 mV to +150 mV, TsdB is redox active between -100 to +300 mV, thus enabling electron transfer between these hemoproteins. The three-dimensional structure of the TsdB-TsdA fusion protein from the purple sulfur bacterium *Marichromatium purpuratum* was solved by X-ray crystallography to 2.75 Å resolution providing insights into internal electron transfer. In the oxidized state, this tetraheme cytochrome *c* contains three hemes with axial His/Met ligation, while heme 3 exhibits the His/Cys coordination typical for TsdA active sites. Interestingly, thiosulfate is covalently bound to Cys³³⁰ on heme 3. In several bacteria including *Allochromatium vinosum*, TsdB is not present, precluding a general and essential role for electron flow. Both, *AvTsdA* and the *MpTsdBA* fusion react efficiently *in vitro* with high potential iron sulfur protein from *A. vinosum* (E_m +350 mV). HiPIP not only acts as direct electron donor to the reaction center in anoxygenic phototrophs but can also be involved in aerobic respiratory chains.

INTRODUCTION

The bifunctional thiosulfate dehydrogenase/tetrathionate reductase TsdA is present in various organisms of different proteobacterial genera (1). In the diheme cytochrome *c* from the purple sulfur bacterium *Allochromatium vinosum* an axial histidine/ cysteine ligation of the central iron atom has been firmly established for the active site heme (2). This type of ligation is rare among prokaryotes,

usually leads to a low redox potential of the corresponding heme (3-6) and appears to be of special importance in sulfur-based energy metabolism. TsdA proteins catalyze the reversible formation of a sulfur-sulfur bond between the sulfane atoms of two thiosulfate molecules, yielding tetrathionate and releasing two electrons. TsdA enzymes of various source organisms exhibit different catalytic bias (7). Whilst the enzyme from the sulfur oxidizer *A. vinosum* is strongly adapted to catalyzing thiosulfate oxidation (2), TsdA from *Campylobacter jejuni* acts primarily as a tetrathionate reductase and enables the organism to use tetrathionate as alternative electron acceptor for anaerobic respiration (8).

At present, it is largely unclear which redox carriers mediate the flow of electrons arising from thiosulfate oxidation into respiratory or photosynthetic electron chains. In several organisms, including *Thiomonas intermedia*, *Sideroxydans lithotrophicus* and *Pseudomonas stutzeri*, *tsdA* is immediately preceded by a gene encoding another diheme cytochrome, TsdB (1). TsdB is not itself reactive with thiosulfate but accepts electrons from TsdA even when TsdA and TsdB do not originate from the same source organism (1). Kinetic data that quantitatively describe the interaction between TsdA and TsdB have not been published so far. In the anoxygenic phototrophic purple sulfur bacterium *Marichromatium purpuratum*, TsdA and TsdB form a fusion protein with TsdB constituting the amino-terminal domain (7). TsdBA fusion proteins are also encoded in other members of the family Chromatiaceae i.e. *Thiorhodococcus* sp. AK35 (D779_1816), *Thiocystis violascens* (Thivi_3993), *Thiorhodococcus drewsii* (ThidrDRAFT_3922) and *Thioflavococcus mobilis* (Thimo_0460). However, TsdBA fusions are not a common trait in purple sulfur bacteria. In *A. vinosum*, a *tsdB* gene is not present (1).

In *A. vinosum*, the protein with the closest relationship to *T. intermedia* or *P. stutzeri* TsdB is Alvin_2879. This cytochrome *c*₄ (previously cytochrome *c*₅₅₃₍₅₅₀₎) is membrane-bound (possibly via the hydrophobic protein Alvin_2880) and has a positive redox potential of +330 mV (9). Another candidate for accepting electrons from TsdA in purple anoxygenic phototrophic bacteria is the high potential iron sulfur protein (HiPIP). *A. vinosum*

and *M. purpuratum* produce HiPIP and as this protein has a quite positive reduction potential (+350 mV (10)) it would be well suited as an electron acceptor for TsdA. This proposal is corroborated by a previous report where a protein preparation with thiosulfate dehydrogenase activity from *A. vinosum* reduced HiPIP *in vitro* (11).

Here, we study Tsd(B)A enzymes from dedicated sulfur oxidizers and characterize in detail the interaction of TsdA with TsdB. Additionally, we pose the question which proteins serve as immediate electron acceptors for either TsdA alone or the TsdBA fusion protein (when present). It is furthermore intended to derive models for the electron flow involved.

RESULTS

Characterization of TsdA and TsdB—UV-vis electronic absorbance spectroscopy, X-ray diffraction and activity assays have revealed a number of characteristic features of AvTsdA (1,2,12). However, the electrochemical window in which the hemes are redox active remained unknown. To gain insight into this property we mapped out the redox activity of AvTsdA adsorbed as an electroactive film on optically transparent mesoporous nanocrystalline SnO₂ electrodes. The spectrum of the enzyme-coated electrode equilibrated at +302 mV contained features typical of ferric *c*-type hemes superimposed on a small contribution from light-scattering by the electrode material (Fig. 1). The Soret maximum at 406 nm and broad lower intensity features in the $\alpha\beta$ -region are typical of those displayed by solutions of oxidized AvTsdA (1). When the electrode potential was lowered to -648 mV in 50 mV steps with a spectrum recorded after a 60 s pause at each desired potential (Fig. 1), those features were replaced with peaks having maxima at 418, 523 and 553 nm, which are typical of dithionite reduced enzyme (1). Variation of the Soret intensity at 418 nm with electrode potential revealed that the hemes were reduced between approximately +150 and -350 mV (Fig. 1 inset, closed squares).

The response of reduced AvTsdA to stepwise increase of the electrode potential was assessed in a similar manner. The potential was raised in 50 mV steps and spectra recorded after a 60 second pause at each potential (Fig. 1 inset, open squares).

Between -648 and -98 mV the variation in Soret intensity with the applied potential was very similar to that recorded on reduction. However, further increase of potential revealed significantly less oxidation than anticipated from the behavior seen on reduction of the enzyme. Importantly, spectra typical of the fully oxidized enzyme were measured after the electrode was poised at +302 mV for approximately 30 min. It was concluded that the electrodic redox cycling of adsorbed AvTsdA was fully reversible but that full reduction occurred more quickly than complete re-oxidation. Further experiments confirmed that this behavior persisted over multiple rounds of reduction and reoxidation. The spectral changes induced by variation of potential between -648 and -98 mV were rapidly reversed and accounted for approximately 35% of the change in absorbance at 418 nm when spectra of the fully oxidized and fully reduced forms of the enzyme were compared. By contrast, variations of electrode potential between -98 and +302 mV showed rapid reduction and much slower reoxidation, and the associated changes in absorbance accounted for approximately 65% of the total seen on full redox cycling of the enzyme. It was concluded that the slow reoxidation associated with higher potential redox event(s) was not a consequence of reversible redox events that occurred at lower potentials. Detailed inspection of the spectra provided no indication for the presence of high-spin ferric- or ferrous-heme.

The hysteretic nature of the plot of absorbance *versus* potential prevented Nernstian analysis to define the heme reduction potentials. Nevertheless, some further conclusions regarding the redox activity of AvTsdA can be proposed in light of the crystal structures reported (2,12). The fully oxidized diheme cytochrome AvTsdA contains His/Cys coordination in heme 1 and His/Lys in heme 2. His/Cys ligated hemes are typically distinguished from other low-spin *c*-type hemes by having much lower reduction potentials and smaller changes in extinction coefficient associated with the Fe(III)/(II) couple (4,13). As a consequence, we propose that reduction of His/Cys ligated heme 1 occurs reversibly between *ca.* -100 and -350 mV. Reduction of His/Lys ligated heme 2 is proposed to occur between *ca.* +150 and -100 mV. AvTsdA X-ray structures reveal that this re-

duction is accompanied by a switch of Lys by Met as axial distal ligand to ferrous-heme 2 (2). Such a change of ligation would be expected to raise the reduction potential of heme 2. If the Met ligand is replaced slowly by Lys upon enzyme oxidation this would account for the hysteretic nature of the redox behavior displayed by AvTsdA.

In contrast to TsdAs, TsdB proteins are not well characterized. The most closely related characterized cytochromes on a sequence level belong to the diheme cytochromes of the c_4 family (1). The recombinant TsdB protein from *T. intermedia* indeed binds two heme groups of 616.5 Da as the mass of 21792.5 Da determined by MALDI-TOF mass spectrometry almost exactly matched the mass of 21783.3 Da predicted for the mature recombinant protein including Strep tag and two hemes. The same held true for recombinant *S. lithotrophicus* TsdB (measured mass: 22864 Da, predicted mass: 22835 Da). UV-Vis spectroscopy of pure recombinant TsdB from *S. lithotrophicus* is shown in Fig. 2. The spectrum conforms to that of *Ti*TsdB (1).

A sequence alignment of various TsdB proteins (Fig. 3) reveals two conserved methionine residues but no conserved histidines or cysteines indicating that both hemes of TsdB have axial coordination by His/Met. This is underpinned by the 700 nm peak in the spectrum, which is characteristic for methionine as the sixth axial heme iron ligand (14) and corroborated by the *Mp*TsdBA crystal structure determined herein (see below). A shift of the Soret band from 411 to 417 nm upon reduction was observed. Moreover, there is a distinct δ band at 359 nm in the oxidized protein spectrum. In the reduced state, the α band was detected at 552 nm and the β band at 523 nm. A split α band characteristic for a number of c_4 -type cytochromes, including those from purple sulfur bacteria, was not observed (9,15). The UV-vis spectrum for oxidized TsdB exhibited a low intensity high spin feature at 620 nm similar to that noted for cytochrome c_4 from *P. stutzeri* (16). Obviously, the ferric form of TsdB holds a small fraction of high-spin heme probably caused by weakening of the Fe-S bond at one of the two hemes with concomitant partial dissociation of the methionine and formation of an Fe-aquo bond just as outlined for the *P. stutzeri* cytochrome (16).

The reduction potential of *Ti*TsdB was determined by potentiometry with a gold electrode (Fig. 4). The potential changes determined upon reduction and reoxidation of TsdB match well. The two hemes are redox active between -100 and +300 mV. Hysteresis was not observed, consistent with both hemes being His/Met ligated. Ligand changes are not apparent.

TsdB is an Electron-Transferring Unit Tightly Interacting with TsdA—The interaction of TsdA and TsdB proteins was analyzed for the recombinant proteins from *S. lithotrophicus*. Upon analytical gel permeation chromatography *SITsdA* alone eluted at a volume corresponding to a molecular mass of 65 kDa, indicating dimerization of the protein under the conditions applied (monomer: 33042 Da). In contrast, *SITsdB* behaved as a 22 kDa monomer (predicted molecular mass: 22835 Da). When both proteins were produced simultaneously in *E. coli* and purified employing the Strep tag attached to TsdA, a preparation was obtained that exhibited two heme stainable polypeptides. In size, these exactly matched *SITsdB* and *SITsdA* (Fig. 5). The co-purification of the two proteins is evidence for significant interaction between them. Upon size exclusion chromatography, *SITsdA* and *SITsdB* co-eluted again in fractions corresponding to a mass of 108 kDa, indicating formation of an $\alpha_2\beta_2$ heterodimer.

Characterization of the TsdBA Fusion Protein from Marichromatium purpuratum—The protein encoded by *tsdB-tsdA* gene fusion in *Marichromatium purpuratum* provides an exceptional possibility to study the complete tetraheme cytochrome for catalytic properties and internal electron transfer. A sequence alignment of *Mp*TsdBA with combined TsdB and TsdA sequences from *S. lithotrophicus* and *T. intermedia* shows significant similarity between the N-terminal region of *Mp*TsdBA and TsdB (aa 1-199 of *Mp*TsdBA and *Ti*TsdB share 45% sequence identity) and between the C-terminal region of *Mp*TsdBA and TsdA (aa 224-518 of *Mp*TsdBA compared to AvTsdA or *Ti*TsdA: 39% and 50% sequence identity, respectively). The heme distal ligands cysteine and methionine of TsdA as well as the two putative heme ligating methionines are strictly conserved (Fig. 3). Therefore, we predicted *Mp*TsdBA to contain three His/Met ligated and one His/Cys ligated heme.

UV-Vis spectroscopy of *MpTsdBA* protein is shown in Fig. 6. The presence of His/Met ligated hemes in *MpTsdBA* is substantiated by the 700 nm peak in the spectrum of the oxidized protein. This absorption band is characteristic for methionine as heme iron ligand (14). A shift of the Soret band from 413 to 420 nm was observed upon reduction. Moreover, there is a distinct δ band at 363 nm in the oxidized protein spectrum. The α band is located at 553 nm, whilst the β band resides at 524 nm. The partly reduced spectrum exhibits a low intensity high spin feature at 620 nm similar to *AvTsdA* (2). The $A_{413\text{nm}}/A_{280\text{nm}}$ for pure oxidized *MpTsdBA* is 3.4.

Crystal Structure Determination and Model Quality of MpTsdBA—To compare structural features of TsdA and TsdBA, to get a closer look into ligation of the four heme groups and to see how TsdA and TsdB domains are linked to each other, we have determined the X-ray structure of *MpTsdBA* by Fe-SAD. Crystals belong to the hexagonal space group *H32* with cell dimensions $a=b=159.75 \text{ \AA}$ and $c=393.09 \text{ \AA}$. There are two molecules in the asymmetric unit corresponding to a Matthews coefficient (17) of $2.8 \text{ \AA}^3 \text{ Da}^{-1}$ and a solvent content around 56%. The “as isolated” structure was refined to 2.75 \AA resolution with R_{cryst} of 15.7% and R_{free} of 19.8% using a 141° -sweep of data with overall better statistics. Data collection and refinement statistics are depicted in Table 3. The high R_{meas} values observed for both sweeps are due, firstly, to the fine binning that *autoPROC* implements during data reduction, and secondly, to the fact that the crystal has some regions in the rotational space that are of bad quality. This is perfectly clear in the plots R_{meas} vs. image number output by *autoPROC* (data not shown), highlighting that the high R_{meas} values are due to the crystal quality and not radiation damage. No evidence for radiation damage is also observed in a $m|F_o|-m|F_c|$ map calculated using both data sweeps (data not shown). *MpTsdBA* is numbered without taking into account its 23-aa signal peptide that is removed upon transport into the periplasm. The model comprises the following residues of the mature recombinant protein: Pro¹-Leu¹⁹¹ and Arg²³⁷-Val⁵¹⁵ (chain A) and Pro¹-Ala¹⁹² and Ala²⁴⁰-Ala⁵¹⁶ (chain B), eight heme molecules, two thiosulfate ions, two chloride ions, seven ethylene glycols,

two 1,2-propanediol and one triethylene glycol, and 113 water molecules. Electron density maps are of good quality except for the C-terminal Histag and the disordered loop connecting TsdB and TsdA domains. This region (45-amino acid residues long in chain A and 47 in chain B) has a predicted loop-like secondary structure and is not included in the final model, since no electron density was observed. Moreover, some parts of the map are somewhat “noisy” with positive and negative difference map peaks in the solvent region that could not be modelled.

Overall Fold and Similar Structures of MpTsdBA—*MpTsdBA* is organized into two domains, an N-terminal TsdB domain and a C-terminal TsdA domain (Fig. 7A). Each domain comprises two subdomains which are related by a pseudo-2-fold symmetry axis. Each subdomain consists of four α -helices surrounding a heme group, the typical class I *c*-type cytochrome topology. This has been previously reported for the *AvTsdA* crystal structure (2,12) and is also observed for the *M. purpuratum* N-terminal TsdB domain. The four subdomains superimpose with r.m.s.d. of 1.3-3.0 \AA for ~ 70 aligned C_α atoms corresponding to sequence similarities between 10-38%.

The final model coordinates were submitted to the DALI server (18), showing no similar structures to the complete *MpTsdBA* arrangement. However, several hits structurally match each domain of the enzyme separately. The highest matches to *MpTsdB* domain were cytochrome *c4* from *Pseudomonas stutzeri* (PDB code: 1M6Z), cytochrome *c552* from *Acidithiobacillus ferrooxidans* (1H1O), the cytochrome subunit of flavocytochrome *c* sulfide dehydrogenase from *A. vinosum* (1FCD), and flavocytochrome *c* from *Thermochromatium tepidum* (3VRD), with Z-scores of 22.7-17.5, r.m.s.d.s of 2.0-2.4 \AA and sequence identities between 30 and 23%.

The highest hit for the *MpTsdA* domain was *AvTsdA* (4V2K, 4WQ9) with a Z-score of 30.6 (with 20% sequence identity and r.m.s.d. of 1.4 and 1.2 \AA , respectively), followed by SoxAX from *Rhodovulum sulfidophilum* (2OZ1), the SoxD subunit of SoxCD from *Paracoccus pantotrophus* (2XTS), and the SoxA subunits of SoxAX from *Starkeya novella* (3OA8) and *P. pantotrophus*

(2C1D). Z-scores ranged from 12-7.4 and r.m.s.d.s from 2.1 to 4.7 Å.

Heme Coordination in the “As Isolated” MpTsdBA—The *MpTsdBA* crystal structure shows four heme groups per chain packed as a wire with closest Fe-to-Fe distances between 15-19 Å and shortest edge-to-edge distances of 3.5 to 6.6 Å (Figs. 7B and 7C). This agrees well with other multiheme cytochrome structures that show edge-to-edge distances of 4 to 8 Å (19,20).

The four hemes are covalently bound to the polypeptide chain through thioether bonds formed by cysteine residues Cys²¹ and Cys²⁴ for heme 1, Cys¹²¹ and Cys¹²⁴ for heme 2, Cys²⁸⁷ and Cys²⁹⁰ for heme 3, and Cys⁴⁰² and Cys⁴⁰⁵ for heme 4 (Fig. 8A-D). Moreover, the structure confirmed the spectroscopic evidence gathered showing that this tetraheme cytochrome *c* has three hemes (hemes 1, 2 and 4) with His/Met coordination (Figs. 8A,B,D). Axial ligation by histidine and cysteine is typical for the active site of TsdA proteins (2,12). Indeed, heme 3 exhibits axial ligation by His²⁹¹ and the S_γ atom of Cys³³⁰ is located in close vicinity to the heme iron such that it could serve as the sixth ligand. However, the 2.9 Å distance between the sulfur and the iron atom precludes direct ligation (8C,E,F). It has been shown earlier that the S_γ atom of the corresponding active site cysteine (Cys⁹⁶) in TsdA from *A. vinosum* can adopt two different conformations by rotation of the cysteine C_α-C_β bond. Thereby, the sulfur atom switches between iron-ligating and iron-non-ligating states (2). The non-ligating conformation has been proposed as an essential intermediate step in the catalytic cycle, possibly involving covalent attachment of a substrate molecule (2,12).

Remarkably, in the “as isolated” structure of *MpTsdBA* a thiosulfate ion is indeed covalently bound to Cys³³⁰. A *polder* map supporting the modelling of the thiosulfate ion is depicted in Fig. 8E. The thiosulfate is oriented such that the S1-S2 plane points towards the heme plane, and the S2 atom lies 2.06 Å away from the S_γ atom of Cys³³⁰, thus being within covalent bond distance. Thiosulfate was refined to 66% occupancy in chain A and 72% in chain B. The S_γ of Cys³³⁰ (full occupancy) superposes well with the S_γ atom of Cys⁹⁶ in AvTsdA with bisulfite (PDB code 4WQB). Here, the S_δ of persulfurated Cys⁹⁶ superimposes with S2

of thiosulfate in the *MpTsdBA* structure. In both structures, these ligand-bound cysteines are not coordinating the heme. Noteworthy, some continuity in the electron density maps is still seen on heme 3, even though Cys³³⁰ is not ligated to the heme iron. We expect *MpTsdBA* Cys³³⁰ to coordinate the heme when no ligand/substrate is present, similar to what is observed in AvTsdA crystal structures (2,12).

The thiosulfate substrate lies in a cleft accessible from the solvent to Cys³³⁰ and heme 3. This cavity is delineated by the side chains of positively charged residues Arg³¹⁴, Lys³¹⁶, Arg³²⁶, Arg⁴³⁸ and Arg⁴⁸⁰ (Fig. 8F), which have been previously proposed to be involved in the orientation and stabilization of the substrate for catalysis (2,12). Some positive electron density ($m/F_o|-D/F_c|$) is present nearby the substrate, although no density is observed in $2m/F_o|-D/F_c|$ maps (even at low contours). This electron density is observed between the N_ε atom of Lys³¹⁶ and the plane formed by the three oxygen atoms of the thiosulfate ion (although independent from the density observed for the thiosulfate ion itself). Since this electron density was not amenable to refinement, nothing was included in the final 3D-structure. Furthermore, heme 3 seems to display another residual conformation with one of the propionates alternating between this cavity and a cleft above the heme plane delineated by Arg³⁷⁷, Arg³⁸¹ and the N main chain atoms of Gly³⁷⁸ and Tyr³⁷⁹. This motion is illustrated by the different conformation modelled for heme 3 in both chains, either pointing towards the active site cavity, in chain A (Fig. 8E), or towards the cleft above the heme plane, in chain B (Figs. 8C and 8F). However, this possible alternate conformation could not be properly refined and therefore it was not added to the crystallographic model.

Reactivity with external electron acceptors—To test different electron acceptors for TsdA and TsdB, we performed enzyme activity assays with TsdB from *T. intermedia*, *A. vinosum* cytochrome *c*₄ (Alvin_2879) and *A. vinosum* HiPIP as electron acceptors. All three potential electron acceptors were produced as recombinant proteins in *E. coli*.

Previously, it had been shown that TsdB from *T. intermedia* is not reactive with thiosulfate but that it is instantaneously reduced when TsdA is

added in the presence of thiosulfate (1). Here, we succeeded in obtaining quantitative kinetic data for a homologous system by analyzing electron transfer between TsdA and TsdB from *S. lithotrophicus*. Just as *TtTsdB*, *STsdB* alone is not reduced by addition of thiosulfate. An enzyme activity assay with *STsdA* as the catalyst and *STsdB* as the electron acceptor resulted in a specific activity of 6.3 U mg^{-1} for *STsdA*. $S_{0.5}$ for thiosulfate was determined to be 0.04 mM . This unambiguously identified *STsdB* as an effective electron acceptor for TsdA from the same organism. However, a heterologous approach yielded a different result: with 0.6 U mg^{-1} the specific activity of *AvTsdA* with TsdB from *T. intermedia* amounted to only one tenth of that determined for the homologous system, whilst $S_{0.5}$ for thiosulfate (0.03 mM) resided in a similar range.

In a further series of experiments, *AvTsdA* activity was tested with Cyt c_4 originating from the same host. It should be noted that the recombinant cytochrome was electrophoretically pure and that it exhibited exactly the same spectral features as Cyt c_4 purified from *A. vinosum* cells including the characteristic split α -band (9). The specific activity of *AvTsdA* with *AvCyt c₄* as the electron acceptor amounted to 0.6 U mg^{-1} and was thus not found to be higher than with TsdB from a different source organism. Therefore, we exclude those diheme cytochromes as efficient electron acceptors for *AvTsdA* *in vitro* as well as *in vivo*.

HiPIP from *A. vinosum*, a protein with a positive reduction potential ($+350 \text{ mV}$ (10)), was tested as another potential candidate for accepting electrons from *AvTsdA* as well as from *MpTsdBA*. Indeed, both thiosulfate dehydrogenases reacted efficiently with *A. vinosum* HiPIP (Fig. 9, Table 4). *AvTsdA* exhibited a higher V_{\max} with HiPIP as electron acceptor, whilst *MpTsdA* featured an especially low $S_{0.5}$ value for thiosulfate when the reaction was measured with HiPIP as electron acceptor. In both cases $S_{0.5}$ for thiosulfate was much lower with HiPIP than with ferricyanide as the electron acceptor indicating cooperativity between the electron-transferring heme 2 and the active site heme 1. *A. vinosum* and *M. purpuratum* both encode HiPIP in their genome and both thiosulfate dehydrogenases exhibit substantial specific activity with HiPIP as electron acceptor *in vitro*, leading us

to conclude that HiPIP also serves as an efficient *in vivo* electron acceptor for Tsd(B)A in both organisms.

DISCUSSION

In our approach to find suitable electron acceptors for TsdA-type thiosulfate dehydrogenases, we first focused on TsdB, a diheme cytochrome encoded upstream of TsdA in a number of different organisms. As demonstrated here for the proteins from *S. lithotrophicus* and earlier for those from *T. intermedia* (1), TsdA and TsdB enzymes interact strongly with each other and form an $\alpha_2\beta_2$ heterodimer. The same arrangement has been described for thiosulfate dehydrogenase from *Halothio-bacillus neapolitanus* (21), which consists of heme *c* binding subunits of 27 and 33 kDa conforming in size with TsdA and TsdB, respectively.

In this work, a redox range of -300 to $+150 \text{ mV}$ was determined for *AvTsdA* whilst *TtTsdB* is redox active between -100 and $+300 \text{ mV}$. Generalizing this finding, we state that the overall reduction potential of TsdB is more positive than that of TsdA which should enable electron flow from TsdA to TsdB. Indeed, reduction of *TtTsdB* by *AvTsdA* had been shown previously (1) and was verified here for the proteins from *S. lithotrophicus*. Enzyme activity assays further revealed *STsdB* as an effective electron acceptor for *STsdA* but not for *AvTsdA*. This was not surprising, as *A. vinosum* does not contain a gene encoding TsdB (Table 5).

In *A. vinosum*, the gene with strongest similarity to *tsdB* is *Alvin_2879*. The encoded high-potential diheme cytochrome c_4 has been suggested to play a role in transferring electrons to the photosynthetic reaction center (9). The *M. purpuratum* genome also encodes a protein (*Marpu_15750*) with high similarity to *A. vinosum* Cyt c_4 (78 % identity on the sequence basis; Table 5). In the anoxygenic phototroph *Rubrivivax gelatinosus* a related cytochrome c_4 indeed has an established function as an alternative electron donor to the photosynthetic reaction center (22). It was therefore feasible to assume that electrons generated by thiosulfate oxidation could be shuttled to the reaction center via cytochrome c_4 in purple sulfur bacteria. However, the very low specific activity of

AvTsdA with *A. vinosum* cytochrome *c*₄ essentially precludes such a role (Fig. 10).

In many anoxygenic photosynthetic bacteria, the periplasmic high potential iron-sulfur protein is well known to shuttle electrons between the cytochrome *bc*₁ complex and the photosynthetic reaction center during cyclic electron flow (23-26). This function has also been firmly established for the protein from *A. vinosum* (24,27). Here, we demonstrate that HiPIP is a suitable electron acceptor for Tsd(B)A from *A. vinosum* and *M. purpuratum* *in vitro*, identifying this protein as the most likely electron carrier between the thiosulfate-oxidizing enzyme and the reaction center during growth in the light. It should be noted that a direct interaction between Tsd(B)A and the photosynthetic reaction center cannot be completely excluded so far.

Many purple sulfur bacteria, including *A. vinosum* are capable of chemolithotrophic growth on reduced sulfur compounds and oxygen under microaerobic conditions (28). Accordingly, *cbb*₃ as well as ubiquinol oxidases are encoded in their genomes. While the standard reduction potential of the thiosulfate/tetrathionate couple (+198 mV, (7)) appears too positive to feed electrons directly into the quinone pool, and from there to oxygen, delivery of electrons originating from the thiosulfate to tetrathionate conversion to *cbb*₃ oxidase is certainly feasible. In fact, HiPIP has been reported to be involved in bacterial respiratory chains (29,30) and is a prime candidate for electron transport between Tsd(B)A and the terminal oxidase in those organisms where it is present. However, in chemotrophs like *T. intermedia* or *S. lithotrophicus* the situation must be different because these bacteria do not contain HiPIP. In fact, for these organisms it is not exactly established so far which periplasmic proteins deliver electrons to *cbb*₃ oxidase, regardless of the electron donor oxidized. For *S. lithotrophicus* it is assumed that the *c*-type cytochrome MtoD (Slit_2498) can transfer electrons stemming from iron oxidation to *cbb*₃ oxidase and the cytochrome *bc*₁ complex (31). In the *T. intermedia* genome there are two *c* type cytochromes (Tint_2575 and Tint_3060) with 36% and 42% sequence identity to *S. lithotrophicus* MtoD, respectively, which may serve a similar function. It may be possible that thiosulfate dehydrogenase

delivers electrons to the MtoD(-like) cytochrome which then shuffles the electrons to the terminal oxidase.

Nevertheless, an alternate scenario is also possible when we consider the similarity between TsdB and cytochromes of the *c*₄ type (about 49% sequence identity between *Ti*TsdB and Cyt *c*₄ from *Achromobacter xylooxidans* or *Pseudomonas protegens*). Cytochromes of the *c*₄-type have been reported to donate electrons to *cbb*₃-type cytochrome *c* oxidases in various oxygen-respiring bacteria (32-34) and we therefore consider the possibility that TsdB serves as a direct electron donor to *cbb*₃ oxidase at least in tetrathionate-forming thiosulfate oxidizers that neither contain HiPIP nor any cytochrome *c*₄ homolog except of TsdB.

We have determined the first three-dimensional structure of *M. purpuratum* TsdBA, where TsdA is fused with its electron acceptor TsdB. It showed heme arrangement with characteristic class I *c*-type cytochrome topology, unveiling their relative heme spatial disposition and providing insights into the electron flow during enzymatic reaction. In the *Mp*TsdBA structure, a thiosulfate ion is covalently bound to S_γ of Cys³³⁰ in heme 3, although the protein was produced in and purified from *E. coli* without the addition of thiosulfate to media or buffers. This implies high affinity of the enzyme to thiosulfate which is possibly present in the complex growth medium in very low concentrations. It should be noted that recombinant AvTsdA and also several SoxA proteins have been isolated with the active site cysteine in a partially or fully persulfurated state (2,35-37). This has been interpreted as indication for temporary binding of thiosulfate and subsequent incomplete catalysis. Just as proposed here, thiosulfate was assumed to originate from the *E. coli* growth medium (2).

Regardless of its source, the covalent attachment of a complete thiosulfate molecule to the *Mp*TsdBA active site cysteine strongly supports the hypothesis that tetrathionate formation from two thiosulfate molecules proceeds via a rhodanese-like reaction mechanism involving a thiosulfate transfer reaction with a thiosulfate molecule covalently bound to the active site cysteine as an essential intermediate in the catalytic cycle (2,12). This type of mechanism has been illustrated

in detail by Grabarczyk et al. (12) for TsdA from *A. vinosum*. A rhodanese-like reaction cycle has also repeatedly been depicted and discussed for the closely related SoxXA protein, but could not be unambiguously proven before (4,35). The MpTsdBA structure provides conclusive evidence that the reactions catalyzed by TsdA as well as SoxXA enzymes indeed involve a cysteine S-thiosulfonate intermediate that is formed once the first thiosulfate molecule is positioned in the substrate binding pocket by positively charged amino acid side chains (Arg³¹⁴, Lys³¹⁶, Arg³²⁶, and Arg⁴³⁸ in MpTsdBA, Fig. 8F). The latter also stabilize the cysteine S-thiosulfonate group once it has formed. Formation of the cysteine S-thiosulfonate releases two electrons which reduce the iron atoms of the two hemes in TsdA to the Fe(II) state. Heme re-oxidation by an external electron acceptor is then likely to be followed by a thiol-disulfide exchange reaction that proceeds via an attack of the sulfane atom of a second thiosulfate molecule on the thiosulfonate group (12).

We conclude that catalysis of thiosulfate oxidation by Tsd(B)A enzymes and very probably also that by SoxXA proteins involves formation of a covalent adduct between the sulfane sulfur atom of thiosulfate and the S_γ of the active site cysteine. When present, TsdB is the immediate electron acceptor of TsdA. TsdB is very likely able to transfer electrons directly to the *cbh*₃ terminal oxidase. In organisms containing HiPIP, this electron carrier is likely to act as an additional shuttle not only between Tsd(B)A and the terminal oxidase during oxygen respiration but also between Tsd(B)A and the photosynthetic reaction center during photolithotrophic growth in the light.

EXPERIMENTAL PROCEDURES

Bacterial Strains, Plasmids and Growth Conditions—Table 1 lists the bacterial strains and plasmids used for this study. *Escherichia (E.) coli* BL21 (DE3) was used for recombinant protein production and was grown in LB medium. *E. coli* DH5α was used for molecular cloning.

Recombinant DNA Techniques—All general molecular genetics techniques were described earlier (38). Restriction enzymes, T4 ligase and *Pfu* DNA polymerase were obtained from Thermo Scientific (Schwerte, Germany) and used accord-

ing to the manufacturer's instructions. Oligonucleotides for cloning were obtained from Eurofins MWG (Ebersberg, Germany).

Construction of Expression Plasmids—*A. vinosum* *tsdA* and *T. intermedia* *tsdB* genes coding for the mature proteins without the signal peptides were amplified and cloned as described earlier (1). The *tsdA* gene (Slit_1878), the *tsdB* gene (Slit_1877) and the *tsdBA* gene combination (Slit_1877-Slit1878) from *Sideroxydans lithotrophicus* ES-1 (ATCC 700298^T) were amplified from genomic DNA with primers Slit1877_fw/Slit1877_rev, Slit1878_fw/Slit1878_rev and Slit1877_fw/Slit1878_rev, respectively. The native signal peptide encoding sequences were included in all three cases. The *tsdBA* gene fusion (Marpu_02550) from *Marichromatium purpuratum* 984 (DSM 1591^T) was amplified without its original signal peptide encoding sequence using primers MarpuDR1194_for/MarpuDR1194_rev. The gene Alvin_2879, encoding a cytochrome *c*₄ with similarity to TsdB was amplified with primers 2879+Sp-for and 2879-rev such that the signal peptide encoding sequence was included. The HiPIP-encoding *hip* (Alvin_2274) gene (39) was amplified without the signal peptide encoding sequence applying primers Alvin2274-C-strep_for/Alvin2274-C-strep_rev. Chromosomal DNA from *A. vinosum* DSM 180^T served as the template. For cloning of *SltsdB*, *SltsdA*, *SltsdB-tsdA* and Alvin_2879, primers included BsaI restriction sites and the digested PCR products were cloned into BsaI digested pASK-IBA3plus (IBA, Göttingen) resulting in vectors pASK-IBA3plus-slit1877, pASK-IBA3plus-slit1878, pASK-IBA3plus-slit1877-slit1878 and pASK-IBA3plus_Alvin_2879. For the cloning of *MptsdBA* into pET-22b(+) (Novagen), the restriction enzymes NdeI and XhoI were used yielding plasmid pET_MarpuDRAFT_1194. Plasmid pET-Alvin2274 was constructed by cloning *Avhip* into a modified pET-22b(+) vector (pET-soxXAK-strep) encoding a C-terminal Strep tag. This vector had previously been constructed in the course of cloning the *A. vinosum* *soxXAK* genes. PCR primers with NdeI (XAK-NdeI-for) and NcoI (XAK-NcoI-rev) sites were used and the resulting fragment was cloned into pET-22b(+). The XbaI/NcoI fragment of the resulting plasmid was cloned into

pASK-IBA3. XbaI and HindIII served for excising the *soxXAK* genes together with the Strep tag encoding sequence. The XbaI/HindIII fragment was cloned between the XbaI and HindIII sites of pET22b(+) giving pET-soxXAK-strep. Replacing the *soxXAK* genes in this construct by *Avhip* yielded *A. vinosum* HiPIP fused to a carboxy-terminal Strep tag.

Overproduction, Purification and Preparation of Recombinant Proteins—*AvTsdA* and *TiTsdB* were produced as described before (1). For production of *S. lithotrophicus* TsdA, *STsdB* and the simultaneous production of *STsdB* and *STsdA* *Escherichia coli* BL21(DE3) cells containing pASK-IBA3plus-slit1877, pASK-IBA3plus-slit1878 or pASK-IBA3plus-slit1877-slit1878 and pEC86 (40) were cultured in 700 ml LB media supplemented with 100 $\mu\text{g ml}^{-1}$ ampicillin and 25 $\mu\text{g ml}^{-1}$ chloramphenicol at 37°C and 180 rpm after inoculation with an overnight pre-inoculum in a (1:50) dilution. At an $\text{OD}_{600\text{nm}}$ of 0.4 to 0.6, 200 ng ml^{-1} anhydrotetracycline were added and the appropriate culture was switched to 25°C and 90 rpm in case of TsdB production. Cells were harvested after 18 h. *MpTsdBA* and HiPIP were produced in *Escherichia coli* BL21(DE3) cells containing pET_MarpuDRAFT_1194 or pET-Alvin2274 and pEC86 (40). After 2% or 0.5% inoculation with a preculture, the cells were grown in 700 ml LB medium containing 100 $\mu\text{g ml}^{-1}$ ampicillin and 25 $\mu\text{g ml}^{-1}$ chloramphenicol at 37°C and 180 rpm. At an $\text{OD}_{600\text{nm}}$ of 0.5 to 0.6 the cultures were switched to 25°C and 120 rpm for about 18 h. For production of *AvCyt c₄* (Alvin_2879), *E. coli* BL21(DE3) cells containing pASK-IBA3plus_Alvin_2879 and pEC86 (40) were cultured in 400 ml LB medium, 100 $\mu\text{g ml}^{-1}$ ampicillin and 25 $\mu\text{g ml}^{-1}$ chloramphenicol at 37°C and 180 rpm after 2% inoculation with a preculture. At $\text{OD}_{600\text{nm}} \sim 0.5$, 200 ng ml^{-1} anhydrotetracycline were added and the culture was switched to 25°C and 90 rpm for 18 h. Harvested cells were resuspended in 100 mM Tris-HCl buffer pH 8.0 containing 150 mM NaCl and lysed by sonication. After removal of insoluble cell material by centrifugation (10,000 g for 25 min at 4°C), *STsdA*, *STsdB*, *STsdB+TsdA*, *A. vinosum* cytochrome *c₄* (Alvin_2879) and *AvTsdA* were purified by Strep-Tactin (IBA, Göttingen, Germany) affinity chromatography according to the

manufacturer's instructions. *MpTsdBA* was purified by nickel-chelate (Qiagen, Hilden, Germany) affinity chromatography according to the manufacturer's instructions and then subjected to a size-exclusion chromatography step performed on a Hi-Load 16/60 Superdex 75 pg column (GE Healthcare) using an ÄKTApurifier system (GE Healthcare). The column was equilibrated with 20 mM Tris-HCl buffer, pH 7.5 and 150 mM NaCl. TsdB and TsdA from *S. lithotrophicus* were analyzed by the same procedure either separately or as a mixture of both proteins. In this case, the Superdex 75 column was equilibrated with 100 mM Tris-HCl buffer, pH 7.5 and 150 mM NaCl. The column was calibrated with the Molecular weight marker kit MW-GF-70 (GE Healthcare). All purified proteins were desalted with 5 ml HiTrap Desalting columns (GE Healthcare) and concentrated with Amicon Ultra-15 centrifugal filter units (Merck Millipore). Recombinant *S. lithotrophicus* proteins were stored in 100 mM sodium acetate buffer pH 5 at -70°C, *A. vinosum* Cyt *c₄* in 20 mM Tris-HCl buffer pH 7.5 at 4°C, *MpTsdBA* in 20 mM Tris-HCl buffer pH 7.5 with 150 mM NaCl at -70°C and HiPIP in 20 mM Tris-HCl pH 7 at 4°C. The concentration of purified proteins was determined with the BCA kit from Pierce (Rockford, USA). For assessment of purity, sodium dodecyl sulfate-polyacrylamide gel electrophoresis (SDS-PAGE) was performed and the proteins visualized either by Coomassie or heme staining techniques.

UV-vis Spectroscopy with TsdA in Solution—UV-vis spectra were recorded between 250 and 750 nm with an Analytik Jena Specord 210 (Analytik Jena, Jena, Germany).

Assay of Thiosulfate Oxidase Activity with Ferricyanide—Thiosulfate-dependent ferricyanide reduction was measured by following the decrease in absorbance at 420 nm ($\epsilon = 1.09 \mu\text{M cm}^{-1}$). Enzyme activity measurements with *AvTsdA* at pH 4 are described in (2). Activity measurements with *MpTsdBA* were performed with 1 mM ferricyanide at 25°C in 100 mM ammonium acetate buffer pH 5.2 with 200 mM NaCl. Assays were started by addition of TsdA and data were recorded in a Specord 210 spectrophotometer (Analytik Jena, Jena, Germany). Activity is expressed as μmol tetrathionate produced per min and mg protein on

the basis of one tetrathionate formed per two ferricyanide reduced. In the case of enzymes that use two molecules of the same substrate (here thiosulfate) primary v versus $[S]$ plots provide the best way to examine the data (41). Data were fitted to the empirical Hill equation (Eq. 1) using Graph Pad Prism (version 6; Graph Pad).

$$v = \frac{V_{\max}[S]^n}{K + [S]^n} \quad (\text{Eq. 1})$$

The Hill equation resembles the classical Henri–Michaelis–Menten equation; however, the n term allows accounting for non-hyperbolic shapes. A substrate concentration $[S]_{0.5}$ can be reported that yields half maximal velocity and is characteristic of the process. The constant K , which is not equivalent to K_m , characterizes enzyme–substrate interaction. The relationship between K and $[S]_{0.5}$ is $K = [S]_{0.5}^n$.

Assay of Thiosulfate Oxidase Activity with HiPIP—For assays of electron transfer from thiosulfate to the electron acceptor HiPIP, 10 μM HiPIP preoxidized with 40 μM ferricyanide were used. The reaction was started by addition of enzyme and followed by the absorbance decrease at 480 nm. A molar extinction coefficient at 480 nm of 10.7 $\text{mM}^{-1} \text{cm}^{-1}$ (10) was used. Measurements with AvTsdA were performed in 100 mM ammonium acetate buffer pH 5 at 30°C and with MpTsdBA in 100 mM ammonium acetate buffer pH 5.2 with 200 mM NaCl at 25°C.

Assay of Thiosulfate Oxidase Activity with TsdB or AvCyt c_4 —Thiosulfate-dependent reduction of *T. intermedia* TsdB or *A. vinosum* Cyt c_4 was measured by following the increase in absorbance at 417 nm ($\epsilon_{\Delta 417\text{nm}} = 99 \text{ mM}^{-1} \text{cm}^{-1}$) for *Ti*TsdB or *Si*TsdB and at 420 nm ($\epsilon_{\Delta 420\text{nm}} = 55 \text{ mM}^{-1} \text{cm}^{-1}$) (9) for AvCyt c_4 . The extinction coefficient for TsdB was calculated with the help of the Beer-Lambert law using distinct concentrations of *Ti*TsdB and the differences in absorbance at 417 nm in the reduced and oxidized spectra. A value averaged from measurements with three different protein concentrations was derived. Assays of *Si*TsdA activity with *Si*TsdB as electron acceptor were carried out in 100 mM ammonium acetate buffer pH 4 at 25°C. AvTsdA activity with *Ti*TsdB was assayed in 100 mM ammonium acetate buffer pH 5 at 30°C, while AvTsdA activity with AvCyt c_4 was

determined in 100 mM ammonium acetate buffer pH 5.5 at 25°C.

Determination of Redox Properties of AvTsdA Adsorbed on a Mesoporous Nanocrystalline SnO₂ Electrode—An optically transparent mesoporous nanocrystalline SnO₂ electrode coated with AvTsdA was prepared using the previously described method (42) with adsorption from a solu-

tion of 10 μM AvTsdA, 2 mM neomycin, 50 mM NaCl, 50 mM HEPES, pH 7. The enzyme-coated electrode was rinsed with 2 mM neomycin, 50 mM NaCl, 50 mM HEPES, pH 7 to remove unbound protein, taken into a N₂-filled chamber (atmospheric O₂ < 2ppm) and immersed in an anaerobic solution of the same composition within a previously described spectroelectrochemical cell (42). The cell was sealed, removed from the anaerobic chamber and inserted into a JASCO V650 UV-visible spectrophotometer thermostated at 4°C and flushed with argon to maintain anaerobicity. Spectral contributions from light scattering by the electrode were minimized by placing a bare SnO₂ electrode (i.e., having no adsorbed enzyme) in the reference beam of the spectrophotometer. The electronic absorbance of the as prepared enzyme-coated electrode revealed features indicative of a mixture of ferric and ferrous hemes. After the electrode had been poised at +302 mV for 45 min the spectrum revealed that the enzyme had been converted to the fully oxidized, all ferric-state. To determine the redox activity of AvTsdA the electrode potential was swept from +302 to -648 mV at a scan rate of 5 mV s^{-1} with a pause of 150 s every

50 mV. At 60 s into each pause a spectrum was measured before the scan continued. Reoxidation of the sample was performed in a similar manner.

Spectra are presented after equating absolute absorbance at 600 nm in order to account for potential dependent changes in the spectral contributions that arise from scattering by the electrode material.

Redox Potentiometry with TsdB in Solution

Measured with a Gold Electrode—The reduction potential of *Ti*TsdB was measured with help of a gold-platinum electrode system under anoxic conditions. The electrode extended into a cuvette containing the protein solution (20 μM) and redox mediators (N,N-dimethyl-1,4-phenylenediamine, p-benzoquinone, trimethylhydroquinone, phenazine, 1,4-naphthoquinone and 1,2-naphthoquinone

at 2 μM each) in 20 mM MOPS buffer pH 6 and was connected to a potentiometer. *Ti*TsdB was reduced by changing the applied potential from -150 mV to 450 mV. Subsequential decrease of the potential again to -150 mV led to reoxidation of the protein. A spectrum was recorded every two minutes and potentials converted to values vs. SHE.

Crystallization, Data Collection, Structure Determination and Refinement—*Mp*TsdBA at a concentration of 3.2 mg ml⁻¹ in 20 mM Bis-Tris-HCl pH 6.5 and 150 mM NaCl was crystallized in 10% (w/v) PEG 8000, 0.1 M Tris-HCl pH 7.0, 0.2 M MgCl₂ and 10 mM trimethylamine hydrochloride (as additive) by vapour-diffusion hanging-drop method at 20°C. Crystallization droplets comprised 1.0 μl of protein, 0.8 μl of precipitant and 0.2 μl of additive, and were equilibrated against a 200 μl of reservoir solution (26% (w/v) PEG 3350). Crystals were cryoprotected with No. 2 solution of CryoProtX screen (Molecular Dimensions), consisting of 25% (v/v) diethylene glycol, 25% (v/v) 1,2-propanediol, and 25% (v/v) glycerol. X-ray diffraction data were collected at a wavelength of 1.7236 Å on beamline ID-29 of the European Synchrotron Radiation Facility (ESRF, Grenoble, France). Data were indexed and integrated with *XDS* (43), space group determined with *POINTLESS* (44) and scaled with *AIMLESS* (45,46), all within *autoPROC* (47) data-processing pipeline. An R_{free} flag was created at this stage corresponding to 5% of the measured reflections of the data set. The structure was determined by single wavelength anomalous dispersion method around the iron edge (Fe-SAD), employing a high multiplicity data collection strategy using the *autoSHARP* module (48), within the *SHARP* package (49). Iterative model building and refinement cycles were performed with *COOT* (50), *BUSTER-TNT* (51), (at early stages of refinement) followed by *phenix.refine* (52), until a complete model was built and refinement convergence achieved. Friedel mates were kept separately and refinement was carried out against I(+)/SIGI(+), I(-)/SIGI(-). A *polder* map (an omit map which excludes the bulk solvent around the omitted region), and $m|F_o|-m|F_c|$ map were calculated within the *PHENIX* package of programs. The Ramachandran diagram was as-

essed with *RAMPAGE* (53) and the model validated with *MolProbity* (54) as implemented in *PHENIX*. All figures were rendered with *PyMOL*, Schrödinger LLC (55).

ACKNOWLEDGEMENTS

The authors acknowledge Isabel Bento and Ana Maria Gonçalves for collecting the X-ray diffraction data. We also acknowledge Susana Gonçalves and ID-29 beamline staff at the European Synchrotron Radiation Facility (ESRF; Grenoble, France) for providing assistance in using the beamline. *S. lithotrophicus* DNA was kindly provided by David Emerson, Bigelow Laboratory for Ocean Sciences, West Boothbay Maine, USA. MALDI-TOF mass spectrometry of *Ti*TsdB and *Si*TsdB was kindly performed by Michaele Josten and Hans Georg Sahl, Institute for Medical Microbiology, Immunology and Parasitology, University of Bonn, Germany. We thank James Durrant (Imperial College London) for the SnO₂ electrodes.

CONFLICT OF INTEREST

The authors declare that they have no conflicts of interest with the contents of this article.

AUTHORS CONTRIBUTIONS

JMK, JAB, JNB, MA and CD wrote the manuscript. CD conceived and coordinated all experiments except the *Mp*TsdBA crystallization and determination of reduction potentials. JMK analyzed and compiled the data for those experiments. JR constructed the vector for production of *Mp*TsdBA and TF the vector for production of HiPIP. AF and JR performed activity assays with *Mp*TsdBA, *Av*TsdA and HiPIP (Fig. 9; Table 4) and recorded UV-vis spectra of *Mp*TsdBA (Fig. 6). TK produced *Av*Cyt c₄ and measured activity of *Av*TsdA with this protein. EK and JMK produced and analyzed proteins from *S. lithotrophicus* (Figs. 2 and 5). KD determined the redox activity of *Ti*TsdB (Fig. 4) under supervision of IACP. SR examined the redox activity of *Av*TsdA (Fig. 1) under supervision of JNB. JAB crystallized *Mp*TsdBA, processed the X-ray data, determined the crystal structure and performed model building and refinement (Figs. 7 and 8; Table 3). JAB and MA analyzed the crystal structure.

REFERENCES

1. Denkmann, K., Grein, F., Zigann, R., Siemen, A., Bergmann, J., van Helmont, S., Nicolai, A., Pereira, I. A. C., and Dahl, C. (2012) Thiosulfate dehydrogenase: a wide-spread unusual acidophilic *c*-type cytochrome. *Environ. Microbiol.* **14**, 2673-2688
2. Brito, J. A., Denkmann, K., Pereira, I. A. C., Archer, M., and Dahl, C. (2015) Thiosulfate dehydrogenase (TsdA) from *Allochromatium vinosum*: structural and functional insights into thiosulfate oxidation. *J. Biol. Chem.* **290**, 9222-9238
3. Pires, R. H., Venceslau, S. S., Morais, F., Teixeira, M., Xavier, A. V., and Pereira, I. A. C. (2006) Characterization of the *Desulfovibrio desulfuricans* ATCC 27774 DsrMKJOP complex - a membrane-bound redox complex involved in the sulfate respiratory pathway. *Biochemistry* **45**, 249-262
4. Bradley, J. M., Marritt, S. J., Kihlken, M. A., Haynes, K., Hemmings, A. M., Berks, B. C., Cheesman, M. R., and Butt, J. N. (2012) Redox and chemical activities of the hemes in the sulfur oxidation pathway enzyme SoxAX. *J. Biol. Chem.* **287**, 40350-40359
5. Reijerse, E. J., Sommerhalter, M., Hellwig, P., Quentmeier, A., Rother, D., Laurich, C., Bothe, E., Lubitz, W., and Friedrich, C. G. (2007) The unusual redox centers of SoxXA, a novel *c*-type heme-enzyme essential for chemotrophic sulfur-oxidation of *Paracoccus pantotrophus*. *Biochemistry* **46**, 7804-7810
6. Kappler, U., Bernhardt, P. V., Kilmartin, J., Riley, M. J., Teschner, J., McKenzie, K. J., and Hanson, G. R. (2008) SoxAX cytochromes, a new type of heme copper protein involved in bacterial energy generation from sulfur compounds. *J. Biol. Chem.* **283**, 22206-22214
7. Kurth, J., Dahl, C., and Butt, J. N. (2015) Catalytic protein film electrochemistry provides a direct measure of the tetrathionate/thiosulfate reduction potential. *J. Am. Chem. Soc.* **137**, 13232-13235
8. Liu, Y.-W., Denkmann, K., Kosciow, K., Dahl, C., and Kelly, D. J. (2013) Tetrathionate stimulated growth of *Campylobacter jejuni* identifies TsdA as a new type of bi-functional tetrathionate reductase that is widely distributed in bacteria. *Mol. Microbiol.* **88**, 173-188
9. Cusanovich, M. A. and Bartsch, R. G. (1969) A high potential cytochrome *c* from *Chromatium vinosum* chromatophores. *Biochim. Biophys. Acta* **189**, 245-255
10. Bartsch, R. G. (1978) Purification of (4Fe-4S)¹⁻²⁻ ferredoxins (high-potential iron-sulfur proteins) from bacteria. *Methods Enzymol.* **53**, 329-340
11. Fukumori, Y. and Yamanaka, T. (1979) A high-potential nonheme iron protein (HiPIP)-linked, thiosulfate-oxidizing enzyme derived from *Chromatium vinosum*. *Curr. Microbiol.* **3**, 117-120
12. Grabarczyk, D. B., Chappell, P. E., Eisel, B., Johnson, S., Lea, S. M., and Berks, B. C. (2015) Mechanism of thiosulfate oxidation in the SoxA family of cysteine-ligated cytochromes. *J. Biol. Chem.* **290**, 9209-9221
13. Du, J., Sono, M., and Dawson, J. H. (2011) The H93G myoglobin cavity mutant as a versatile scaffold for modeling heme iron coordination structures in protein active sites and their characterization with magnetic circular dichroism spectroscopy. *Coord. Chem. Rev.* **255**, 700-716
14. Miles, C. S., Manson, F. D. C., Reid, G. A., and Chapman, S. K. (1993) Substitution of a haem-iron axial ligand in flavocytochrome *b₂*. *Biochim. Biophys. Acta* **1202**, 82-86
15. Branca, R. M. M., Bodó, G., Várkonyi, Z., Debreczeny, M., Ösz, J., and Bagyinka, C. (2007) Oxygen and temperature-dependent structural and redox changes in a novel cytochrome *c₄* from the purple sulfur bacterium *Thiocapsa roseopersicina*. *Arch. Biochem. Biophys.* **467**, 174-184
16. Nissum, M., Karlsson, J.-J., Ulstrup, J., Jensen, P. W., and Smulevich, G. (1997) Resonance Raman characterization of the di-heme protein cytochrome *c₄* from *Pseudomonas stutzeri*. *J. Biol. Inorg. Chem.* **2**, 302-307
17. Matthews, B. W. (1968) Solvent content of protein crystals. *J. Mol. Biol.* **33**, 491-497
18. Holm, L. and Rosenström, P. (2010) Dali server: conservation mapping in 3D. *Nucleic Acids Res.* **38**, W545-W549
19. Igarashi, N., Moriyama, H., Fujiwara, T., Fukumori, Y., and Tanaka, N. (1997) The 2.8 Å structure of hydroxylamine oxidoreductase from a nitrifying chemoautotrophic bacterium, *Nitrosomonas europaea*. *Nat. Struct. Biol.* **4**, 276-284

20. Taylor, P., Pealing, S. L., Reid, G. A., Chapman, S. K., and Walkinshaw, M. D. (1999) Structural and mechanistic mapping of a unique fumarate reductase. *Nat. Struct. Biol.* **6**, 1108-1112
21. Visser, J. M., de Jong, G. A. H., Robertson, L. A., and Kuenen, J. G. (1996) Purification and characterization of a periplasmic thiosulfate dehydrogenase from the obligately autotrophic *Thiobacillus* sp. W5. *Arch. Microbiol.* **166**, 372-378
22. Ohmine, M., Matsuura, K., Shimada, K., Alric, J., Verméglio, A., and Nagashima, K. V. (2009) Cytochrome *c*₄ can be involved in the photosynthetic electron transfer system in the purple bacterium *Rubrivivax gelatinosus*. *Biochemistry* **48**, 9132-9139
23. Bartsch, R. G. (1991) The distribution of soluble metallo-redox proteins in purple phototrophic bacteria. *Biochim. Biophys. Acta* **1058**, 28-30
24. Kennel, S. J., Bartsch, R. G., and Kamen, M. D. (1972) Observations on light-induced oxidation reactions in the electron transport system of *Chromatium*. *Biophys. J.* **12**, 882-896
25. Nagashima, K. V., Matsuura, K., Shimada, K., and Verméglio, A. (2002) High-potential iron-sulfur protein (HiPIP) is the major electron donor to the reaction center complex in photosynthetically growing cells of the purple bacterium *Rubrivivax gelatinosus*. *Biochemistry* **41**, 14028-14032
26. Lieutaud, C., Nitschke, W., Verméglio, A., Parot, P., and Schoepp-Cothenet, B. (2003) HiPIP in *Rubrivivax gelatinosus* is firmly associated to the membrane in a conformation efficient for electron transfer towards the photosynthetic reaction centre. *Biochim. Biophys. Acta* **1557**, 83-90
27. Verméglio, A., Li, J., Schoepp-Cothenet, B., Pratt, N., and Knaff, D. B. (2002) The role of high-potential iron protein and cytochrome *c*₈ as alternative electron donors to the reaction center of *Chromatium vinosum*. *Biochemistry* **41**, 8868-8875
28. Kämpf, C. and Pfennig, N. (1980) Capacity of Chromatiaceae for chemotrophic growth. Specific respiration rates of *Thiocystis violacea* and *Chromatium vinosum*. *Arch. Microbiol.* **127**, 125-135
29. Hochkoeppler, A., Jenney, F. E., Lang, S. E., Zannoni, D., and Daldal, F. (1995) Membrane-associated cytochrome *c*(y) of *Rhodobacter capsulatus* is an electron carrier from the cytochrome bc(1) complex to the cytochrome *c* oxidase during respiration. *J. Bacteriol.* **177**, 608-613
30. Bonora, P., Principi, I., I, Monti, B., Ciurli, S., Zannoni, D., and Hochkoeppler, A. (1999) On the role of high-potential iron-sulfur proteins and cytochromes in the respiratory chain of two facultative phototrophs. *Biochim. Biophys. Acta* **1410**, 51-60
31. Beckwith, C. R., Edwards, M. J., Lawes, M., Shi, L., Butt, J. N., Richardson, D. J., and Clarke, T. A. (2015) Characterization of MtoD from *Sideroxydans lithotrophicus*: a cytochrome *c* electron shuttle used in lithoautotrophic growth. *Front Microbiol.* **6**, 332
32. Arai, H., Kawakami, T., Osamura, T., Hirai, T., Sakai, Y., and Ishii, M. (2014) Enzymatic characterization and in vivo function of five terminal oxidases in *Pseudomonas aeruginosa*. *J. Bacteriol.* **196**, 4206-4215
33. Barco, R. A., Emerson, D., Sylvan, J. B., Orcutt, B. N., Jacobson Meyers, M. E., Ramirez, G. A., Zhong, J. D., and Edwards, K. J. (2015) New insight into microbial iron oxidation as revealed by the proteomic profile of an obligate iron-oxidizing chemolithoautotroph. *Appl. Environ. Microbiol.* **81**, 5927-5937
34. Chang, H. Y., Ahn, Y., Pace, L. A., Lin, M. T., Lin, Y. H., and Gennis, R. B. (2010) The diheme cytochrome *c*₄ from *Vibrio cholerae* is a natural electron donor to the respiratory *cbb*₃ oxygen reductase. *Biochemistry* **49**, 7494-7503
35. Bamford, V. A., Bruno, S., Rasmussen, T., Appia-Ayme, C., Cheesman, M. R., Berks, B. C., and Hemmings, A. M. (2002) Structural basis for the oxidation of thiosulfate by a sulfur cycle enzyme. *EMBO J.* **21**, 5599-5610
36. Dambe, T., Quentmeier, A., Rother, D., Friedrich, C., and Scheidig, A. J. (2005) Structure of the cytochrome complex SoxXA of *Paracoccus pantotrophus*, a heme enzyme initiating chemotrophic sulfur oxidation. *J. Struct. Biol.* **152**, 229-234
37. Kilmartin, J. R., Maher, M. J., Krusong, K., Noble, C. J., Hanson, G. R., Bernhardt, P. V., Riley, M. J., and Kappler, U. (2011) Insights into structure and function of the active site of SoxAX cytochromes. *J. Biol. Chem.* **286**, 24872-24881
38. Dahl, C., Schulte, A., Stockdreher, Y., Hong, C., Grimm, F., Sander, J., Kim, R., Kim, S.-H., and Shin, D. H. (2008) Structural and molecular genetic insight into a wide-spread bacterial sulfur oxidation pathway. *J. Mol. Biol.* **384**, 1287-1300

39. Brüser, T., Trüper, H. G., and Dahl, C. (1997) Cloning and sequencing of the gene encoding the high potential iron-sulfur protein (HiPIP) from the purple sulfur bacterium *Chromatium vinosum*. *Biochim. Biophys. Acta* **1352**, 18-22
40. Arslan, E., Schulz, H., Zufferey, R., Kunzler, P., and Thöny-Meyer, L. (1998) Overproduction of *Bradyrhizobium japonicum* c-type cytochrome subunits of the *cbb₃* oxidase in *Escherichia coli*. *Biochem. Biophys. Res. Commun.* **251**, 744-747
41. Segel, I. H. (1993) *Enzyme kinetics: behaviour and analysis of rapid equilibrium and steady-state enzyme systems*, Wiley-Interscience, New York
42. Marritt, S. J., Kemp, G. L., Xiaoe, L., Durrant, J. R., Cheesman, M. R., and Butt, J. N. (2008) Spectroelectrochemical characterization of a pentaheme cytochrome in solution and as electrocatalytically active films on nanocrystalline metal-oxide electrodes. *J. Am. Chem. Soc.* **130**, 8588-8589
43. Kabsch, W. (2010) XDS. *Acta Crystallogr. D Biol. Crystallogr.* **66**, 125-132
44. Evans, P. R. (2011) An introduction to data reduction: space-group determination, scaling and intensity statistics. *Acta Crystallogr. D Biol. Crystallogr.* **67**, 282-292
45. Evans, P. (2006) Scaling and assessment of data quality. *Acta Crystallogr. D Biol. Crystallogr.* **62**, 72-82
46. Evans, P. R. and Murshudov, G. N. (2013) How good are my data and what is the resolution? *Acta Crystallogr. D Biol. Crystallogr.* **69**, 1204-1214
47. Vornrhein, C., Flensburg, C., Keller, P., Sharff, A., Smart, O., Paciorek, W., Womack, T., and Bricogne, G. (2011) Data processing and analysis with the autoPROC toolbox. *Acta Crystallogr. D Biol. Crystallogr.* **67**, 293-302
48. Vornrhein, C., Blanc, E., Roversi, P., and Bricogne, G. (2007) Automated structure solution with autoSHARP. *Methods Mol. Biol.* **364**, 215-230
49. de la Fortelle, E. and Bricogne, G. (1997) Maximum-likelihood heavy-atom parameter refinement for multiple isomorphous replacement and multiwavelength anomalous diffraction methods. *Meth. Enzymol.* **276**, 472-494
50. Emsley, P., Lohkamp, B., Scott, W. G., and Cowtan, K. (2010) Features and development of Coot. *Acta Crystallogr. D Biol. Crystallogr.* **66**, 486-501
51. Blanc, E., Roversi, P., Vornrhein, C., Flensburg, C., Lea, S. M., and Bricogne, G. (2004) Refinement of severely incomplete structures with maximum likelihood in BUSTER-TNT. *Acta Crystallogr. D Biol. Crystallogr.* **60**, 2210-2221
52. Afonine, P. V., Grosse-Kunstleve, R. W., Echols, N., Headd, J. J., Moriarty, N. W., Mustyakimov, M., Terwilliger, T. C., Urzhumtsev, A., Zwart, P. H., and Adams, P. D. (2012) Towards automated crystallographic structure refinement with phenix.refine. *Acta Crystallogr. D Biol. Crystallogr.* **68**, 352-367
53. Lovell, S. C., Davis, I. W., Arendall, W. B., III, de Bakker, P. I., Word, J. M., Prisant, M. G., Richardson, J. S., and Richardson, D. C. (2003) Structure validation by C α geometry: phi, psi and C β deviation. *Proteins* **50**, 437-450
54. Chen, V. B., Arendall, W. B., III, Headd, J. J., Keedy, D. A., Immormino, R. M., Kapral, G. J., Murray, L. W., Richardson, J. S., and Richardson, D. C. (2010) MolProbity: all-atom structure validation for macromolecular crystallography. *Acta Crystallogr. D Biol. Crystallogr.* **66**, 12-21
55. Delano, W. L. (2002) *The PyMOL molecular graphics system*, DeLano Scientific, San Carlos, California, USA
56. Hanahan, D. (1983) Studies on transformation of *Escherichia coli* with plasmids. *J. Mol. Biol.* **166**, 557-580
57. Karplus, P. A. and Diederichs, K. (2012) Linking crystallographic model and data quality. *Science* **336**, 1030-1033

FIGURE LEGENDS

FIGURE 1. Redox activity of AvTsdA adsorbed on a mesoporous nanocrystalline SnO₂ electrode. Electronic absorbance recorded with the electrode poised at +302 mV (black), +152 to -298 mV at 50 mV intervals (gray) and -648 mV (red). All potentials are quoted *versus* the standard hydrogen electrode (SHE). The arrows indicate increases in absorbance as the electrode potential was lowered. *Inset* shows the normalized change in absorbance at 418 nm against the applied potential as the enzyme was reduced (closed squares) and re-oxidized (open squares).

FIGURE 2. UV-vis spectra of TsdB from *S. lithotrophicus*. As the protein is partly reduced in the “as isolated” state, up to 170 μ M ferricyanide were added to record the oxidized spectrum (black line). For full reduction of the protein Na-dithionite was added (grey line). 100 mM Tris buffer pH 8.0 with 150 mM NaCl and 2.5 mM desthiobiotin was used and spectra are normalized to 750 nm. The oxidized spectrum exhibits a 700 nm peak indicating methionine as heme iron ligand. Protein concentration: 21 μ M in the overview and 94 μ M in the blow-up.

FIGURE 3. Sequence alignment of MpTsdBA and STsdB+TsdA as well as STsdB+TsdA. Sequence comparison of TsdBA fusion protein of *M. purpuratum* (MARPU_02550) with the combined sequence of TsdB and TsdA from *S. lithotrophicus* (Slit_1877 and Slit_1878) and *T. intermedia* (Tint_1893 and Tint_2892). All signal peptide sequences were removed. Heme binding motifs are indicated by grey boxes, putative distal heme ligands are marked by black edging. Strictly conserved residues are marked with asterisks. TsdA sequences of *S. lithotrophicus* and *T. intermedia* start after the gap at amino acids 195 and 189, respectively.

FIGURE 4. Determination of TsdB reduction potential by potentiometry with a gold electrode. Potentiometric determination of redox potentials of both TsdB hemes. Applied potential according to normalized values of the α -peak (553 nm) is shown. Reduction of TsdB (black diamonds) and re-oxidation of the protein (grey squares) was measured. 10 μ M of TsdB in phosphate buffer pH 5.0 was used.

FIGURE 5. Analysis of purified STsdA and STsdB+A by SDS polyacrylamide gel electrophoresis. 10-15 μ g STsdA and STsdB+A obtained after Strep tag affinity chromatography were loaded per lane of a 12.5 % gel and stained for presence of heme. In case of STsdB+A both proteins were produced simultaneously in *E. coli* and purified on the basis of a Strep tag attached to TsdA.

FIGURE 6. UV-vis spectra of MpTsdBA. As the protein is slightly reduced in the “as isolated” state, 60 μ M ferricyanide were added to record the oxidized spectrum (black line). For partial (grey broken line) and full reduction (grey line) of the protein, 0.33 mM and 5 mM Na-dithionite were added, respectively. 100 mM ammonium acetate buffer pH 5 with 200 mM NaCl was used and spectra are normalized to 750 nm. The oxidized spectrum exhibits a 700 nm peak indicating methionine as heme iron ligand and the partially reduced protein exhibits a feature at 630 nm. Protein concentration: 3.3 μ M.

FIGURE 7. X-ray structure of MpTsdBA and heme arrangement. A) Overall fold with TsdB N-terminal domain (residues 1-193) depicted in blue and TsdA C-terminal domain (residues 240-516) in red; the two shades in each domain represent the respective sub-domains (1-90 and 91-193 for TsdB, and 240-377 and 378-516 for TsdA). The heme prosthetic groups are colored by atom type (orange or yellow for carbon, blue for nitrogen, red for oxygen and dark red for iron), B) Fe-to-Fe distances, and C) Closest edge-to-edge distances.

FIGURE 8. Heme coordination of “as isolated” *MpTsdBA* (PDB code 5LO9). A) Heme 1 is coordinated by His²⁵ and Met⁶⁵, B) Heme 2 is coordinated by His¹²⁵ and Met¹⁶⁷, C) Heme 3 is ligated to His²⁹¹ but not to Cys³³⁰. The distance of S_γ to the heme iron is 2.9 Å and thus not close enough for direct ligation. Thiosulfate covalently bound to S_γ of Cys³³⁰ is not shown here for clarity. Presence of thiosulfate is illustrated in detail in panels E and F. D) Heme 4 is ligated by His⁴⁰⁶ and Met⁴⁵⁰, E) Heme 3 with S_γ of Cys³³⁰ covalently bound to thiosulfate, displayed in ball and stick, and *polder* map electron density contoured at 6σ level depicted as a black mesh, and F) Heme 3 in a similar view as in E) but with positively charged residues surrounding the substrate cleft depicted in sticks. Cartoon representation is shown in pale grey with heme moieties and coordinating amino acid residues shown in sticks; color code as in Fig. 7 with sulfur atoms in green.

FIGURE 9. Thiosulfate oxidation catalyzed by *AvTsdA* and *MpTsdBA* with HiPIP as electron acceptor. Enzyme assays with *AvTsdA* were performed in 100 mM ammonium acetate buffer pH 5 at 30°C with 8 nM enzyme. Activity measurements with *MpTsdBA* were performed in 100 mM ammonium acetate buffer pH 5.2 with 200 mM NaCl at 25°C and with 3.9 nM enzyme. In both assays 10 μM HiPIP and 40 μM ferricyanide were used. A change in absorbance was measured at 480 nm. v versus [S] plots were fitted to the Hill equation.

FIGURE 10. Role of periplasmic electron transfer proteins in aerobic respiration or photosynthesis of *A. vinosum*, *M. purpuratum*, *S. lithotrophicus* and *T. intermedia*. All organisms contain genes for NuoA-N (Alvin_2418-2430 +Alvin_2412, Marpu_04365-04430, Slit_1070-1083, Tint_2255-2268), the cytochrome *bc*₁ complex (Alvin_0068-0070, Marpu_01465-01475, Slit_0130-0132, Tint_2192-2194) and *cbb*₃ oxidase (Alvin_0781-0784, Marpu_02795-02810, Slit_0411-0414, Tint_1070-1073). Moreover, *A. vinosum* and *M. purpuratum* can gain energy by photosynthetic growth. HiPIP can transfer electrons to the photosynthetic reaction center (23,24) as well as to *cbb*₃ oxidase (29,30). Cytochrome *c*₄ also is known to transfer electrons to the photosynthetic reaction center (22) as well as to *cbb*₃ oxidase (32-34) in some bacteria. For *S. lithotrophicus* it is assumed that MtoD (Slit_2498) can transfer electrons to *cbb*₃ oxidase and the cytochrome *bc*₁ complex (31).

TABLE 1. *E. coli* strains and plasmids used in this study

Strains and plasmids	Description	Reference or source
Strains		
<i>E. coli</i> DH5 α	F ϕ 80d <i>lacZ</i> Δ M15 Δ (<i>lacZYA-argF</i>) <i>U169 recA1 endA1 hsdR17</i> (rk ⁻ mk ⁺) <i>supE44 λ thi-1 gyrA relA1</i>	(56)
<i>E. coli</i> BL21 (DE3)	F ⁻ <i>ompT hsdS_B</i> (r _B m _B) <i>gal dcm met</i> (DE3)	Novagen
Plasmids		
pEC86	Cm ^r , product from pEC66 and pACYC184 with <i>E. coli ccmABCDEFGH</i> genes	(40)
pET-22b (+)	Ap ^r , T7 promoter, lac operator, C-terminal His tag, pelB leader	Novagen
pASK-IBA3 plus	Ap ^r , <i>tetA</i> promoter/operator, C-terminal Strep tag	IBA (Göttingen)
pET_MarpuDRAFT_1194	Ap ^r , <i>tsdA</i> from <i>M. purpuratum</i> (Marpu_02550) was cloned into pET-22b (+)with Nde I and XhoI, C-terminal His tag	Kurth et al., 2015
pASK-IBATint_ <i>tsdB</i>	Ap ^r ; <i>tsdB</i> from <i>T. intermedia</i> cloned into pASK-IBA3 plus with BsaI, C-terminal Strep tag	(1)
pASK-IBA3plus- <i>slit1877</i>	Ap ^r ; <i>tsdB</i> from <i>S. lithotrophicus</i> (Slit_1877) cloned into pASK-IBA3 plus with BsaI, C-terminal Strep tag	This study
pASK-IBA3plus- <i>slit1878</i>	Ap ^r ; <i>tsdA</i> from <i>S. lithotrophicus</i> (Slit_1878) cloned into pASK-IBA3 plus with BsaI, C-terminal Strep tag	This study
pASK-IBA3plus- <i>slit1877-slit1878</i>	Ap ^r ; <i>tsdBA</i> from <i>S. lithotrophica</i> (Slit_1877-Slit_1878) cloned into pASK-IBA3 plus with BsaI, C-terminal Strep tag	This study
pET-soxXAK-strep	Ap ^r , <i>soxXAK</i> including fragment cloned into pET-22b(+) together with C terminal Strep tag by use of XbaI and HindIII	This study
pET-Alvin2274-C-strep	Ap ^r , <i>hip</i> gene coding for HiPIP from <i>A. vinosum</i> (Alvin_2274) cloned into pET-soxXAK-strep with NdeI and NcoI, C-terminal Strep tag	This study
pPR-IBAAvtsdA	Ap ^r ; <i>tsdA</i> from <i>A. vinosum</i> (Alvin_0091) cloned into pASK-IBA3, C-terminal Strep tag	(1)
pASK-IBA3plus_Alvin_2879	Ap ^r ; Alvin_2879 from <i>A. vinosum</i> cloned into pASK-IBA3 plus with BsaI, C-terminal Strep tag	This study

TABLE 2. Primers used in this study

Primer	Sequence 5'-3'	Reference
MarpuDR1194_for	CGGAGGGATCCTCATATGACGCATCTC	This study
MarpuDR1194_rev	GACCTGCTCGAGATCCTTGGC	This study
Slit1877_fw	ATGGTAGGTCTCAAATGAAGCAAATATTACTAGCAGCATTAAAC	This study
Slit1877_rev	ATGGTAGGTCTCAGCGCTTTTCTGGTTTCCATTGGTTGATTGT	This study
Slit1878_fw	ATGGTAGGTCTCAAATGAAGAATCCCATCGCTATCGCCAT	This study
Slit1878_rev	ATGGTAGGTCTCAGCGCTCTTTGCTGCAGTCTGGTGCTTTC	This study
XAK-NdeI-for	GGAGATTTTCATATGCCGTTGAACGTCTCACACCG	This study
XAK-NcoI-rev	ATGGCTCCATGGTATCGAGACCGATCGAGC	This study
Alvin2274-C-strep_for	GCCCATATGTCCGCTCCCGCCAAT	This study
Alvin2274-C-strep_rev	CAACGGCCCATGGCCGGCCTTCAG	This study
2879+Sp-for	ATGGTAGGTCTCAAATGAAGAAGACTTGGCTGACAACGGT	This study
2879-rev	ATGGTAGGTCTCAGCGCTCTTCGACAGGCCCTGGATGTAC	This study

TABLE 3. Data reduction and refinement statistics for *MpTsdBA* structure

	142.65°-sweep data set (Refinement)	Full 360° data set (Fe-SAD phasing)
PDB ID	5LO9	-
Data collection		
Synchrotron	ESRF (Grenoble - France)	
Beamline	ID-29	
Wavelength (Å)	1.7236	
Space group	<i>H32</i>	
Unit cell		
<i>a, b, c</i> (Å)	159.75, 159.75, 393.09	159.89, 159.89, 392.99
<i>α, β, γ</i> (°)	90.0, 90.0, 120.0	
Resolution range ^a (Å)	113.13 - 2.75 (2.76 - 2.75)	130.99 - 2.82 (2.83 - 2.82)
Total No. of reflections	377526 (2187)	891650 (6064)
No. of unique reflections	50199 (461)	49983 (442)
Completeness (%)	99.0 (87.8)	99.6 (94.2)
Anomalous completeness (%)	98.7 (84.8)	99.6 (94.1)
Multiplicity	7.5 (4.7)	19.0 (13.7)
Anomalous multiplicity	3.9 (2.5)	9.9 (7.0)
$\langle I/\sigma(I) \rangle$	14.9 (2.0)	15.4 (2.4)
R_{meas} (%)	11.7 (70.6)	25.5 (184.7)
R_{pim} (%)	5.7 (41.8)	8.1 (69.2)
$CC_{1/2}$ ^c (%)	99.7 (63.8)	99.4 (75.7)
Refinement		
R_{cryst} ^d (%)	15.7 (25.9)	
R_{free} ^e (%)	19.8 (30.0)	
No. of non-H atoms		
Protein	7028	
Ligands	330	
Waters	113	
R.m.s.d. bonds (Å) ^f	0.013	
R.m.s.d. angles (°)	1.50	
Protein residues	Pro ¹ -Leu ¹⁹¹ and Arg ²³⁷ -Val ⁵¹⁵ (chain A) Pro ¹ -Ala ¹⁹² and Ala ²⁴⁰ -Ala ⁵¹⁶ (chain B)	
Ramachandran plot		
Most favored (%)	97.6	
Allowed (%)	2.4	
Outliers (%)	0	
Rotamer outliers (%)	0.9	
Clashscore	2.69	
<i>MolProbity</i> score ^g	1.28	
B-factors (Å²)		
Protein	52.04	
Ligands/ions	50.43	
Waters	45.06	

^a Information in parenthesis refers to the last resolution shell

^b $R_{\text{meas}} = \sum_h \sum_i |\mathbf{I}_{hi} - \langle \mathbf{I}_h \rangle| / \sum_h \sum_i \langle \mathbf{I}_h \rangle$, where \mathbf{I}_{hi} is the *i*th observation of reflection *h* and $\langle \mathbf{I}_h \rangle$

^c $CC_{1/2}$ ^{*} as described in (57)

^d $R_{\text{cryst}} = \sum_h |\mathbf{F}_{\text{obs}(h)}| - |\mathbf{F}_{\text{cal}(h)}| / \sum_h |\mathbf{F}_{\text{obs}(h)}|$, where $\mathbf{F}_{\text{obs}(h)}$ and $\mathbf{F}_{\text{cal}(h)}$ are the observed and calculated structure factors for reflection *h*, respectively.

^e R_{free} was calculated as R_{factor} but using only 5% of reflections randomly selected and omitted from refinement

^f R.m.s.d., root mean square deviation

^g *MolProbity* score provides a single number that represents the central *MolProbity* protein quality statistics; it is a log-weighted combination of clashscore, Ramachandran not favored and bad side-chain rotamers, giving one number that reflects the crystallographic resolution at which those values would be expected.

TABLE 4: Thiosulfate oxidation of *Av*TsdA and *Mp*TsdBA with ferricyanide and HiPIP

Enzyme assays with *Av*TsdA were performed in 100 mM ammonium acetate buffer pH 4 at 30°C with 8 nM enzyme. Activity measurements with *Mp*TsdBA were performed in 100 mM ammonium acetate buffer pH 5.2 with 200 mM NaCl at 25°C and with 3.9 nM enzyme. In assays with HiPIP as electron acceptor 10 μ M HiPIP and 40 μ M ferricyanide were used and absorbance at 480 nm was followed. In activity assays with ferricyanide as electron acceptor 1 mM ferricyanide was used and the absorbance at 420 nm was measured. The units for V_{max} are μ mol min^{-1} mg protein $^{-1}$. v versus [S] plots were fitted to the Hill equation.

Electron acceptor	Enzyme	V_{max} [U mg $^{-1}$]	$S_{0.5}$ [μ M]	k_{cat} [s $^{-1}$]	$k_{cat}/S_{0.5}$ [mM $^{-1}$ s $^{-1}$]
ferricyanide	<i>Av</i> TsdA	31419 \pm 2408	835 \pm 119	14091	16875
	<i>Mp</i> TsdBA	3011 \pm 108	179 \pm 21	2794	15611
HiPIP	<i>Av</i> TsdA	96 \pm 3	27 \pm 2	43	1595
	<i>Mp</i> TsdBA	26 \pm 1	6 \pm 0	24	4000

TABLE 5.**Occurrence of genes encoding TsdA and putative electron acceptors in the genome sequenced organisms relevant to this study**

Organism	TsdA	TsdB	Cyt c₄	HiPIP
<i>Allochromatium vinosum</i> DSM 180 ^T	Alvin_0091	-	Alvin_2879	Alvin_2274
<i>Marichromatium purpuratum</i> 984 (DSM 1591 ^T)	Marpu_02550		Marpu_15750	Marpu_11560
<i>Sideroxydans lithotrophicus</i> ES-1 (ATCC 700298 ^T)	Slit_1878	Slit_1877	-	-
<i>Thiomonas intermedia</i> K12 (DSM 18155 ^T)	Tint_2892	Tint_2893	-	-

Figure 1

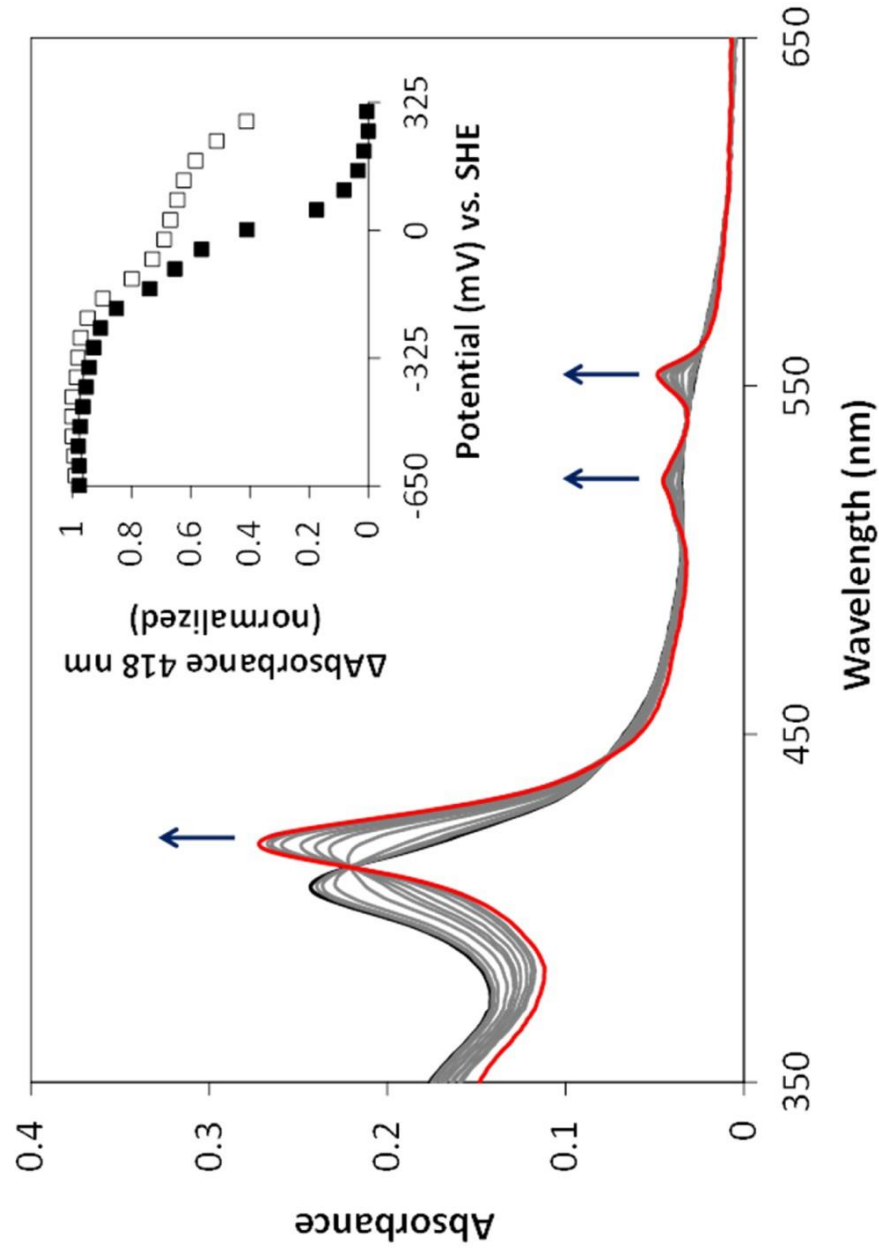


Figure 2

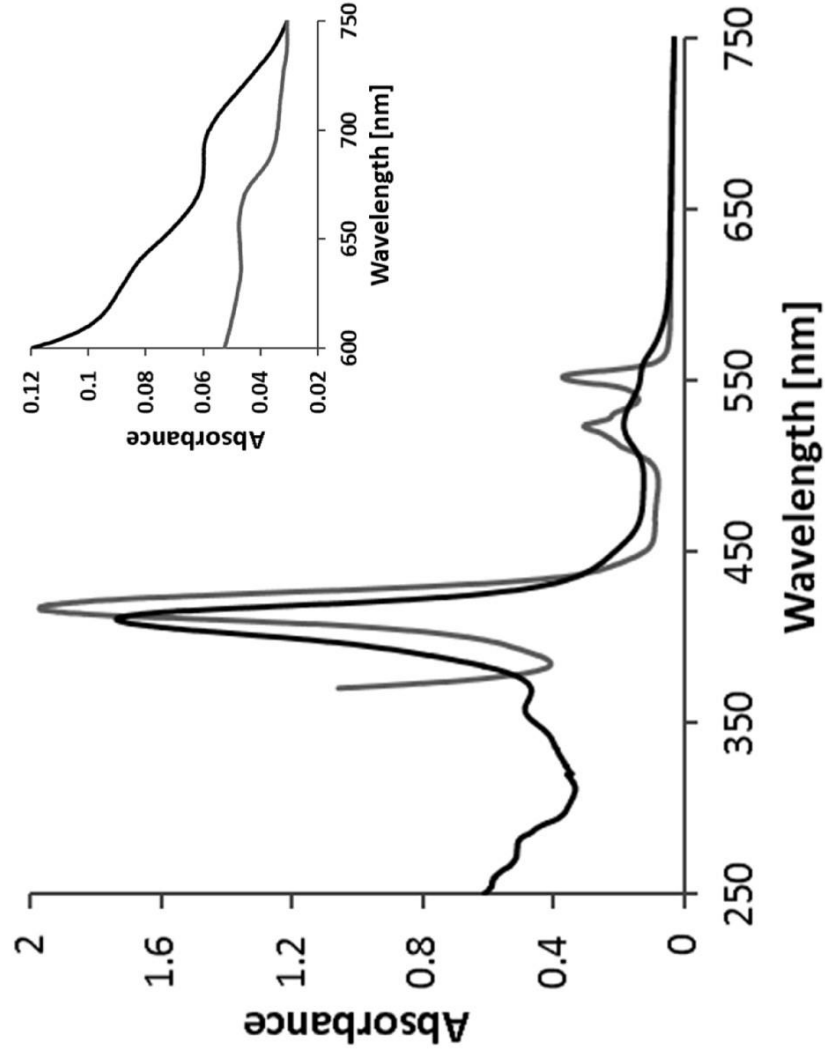


Figure 4

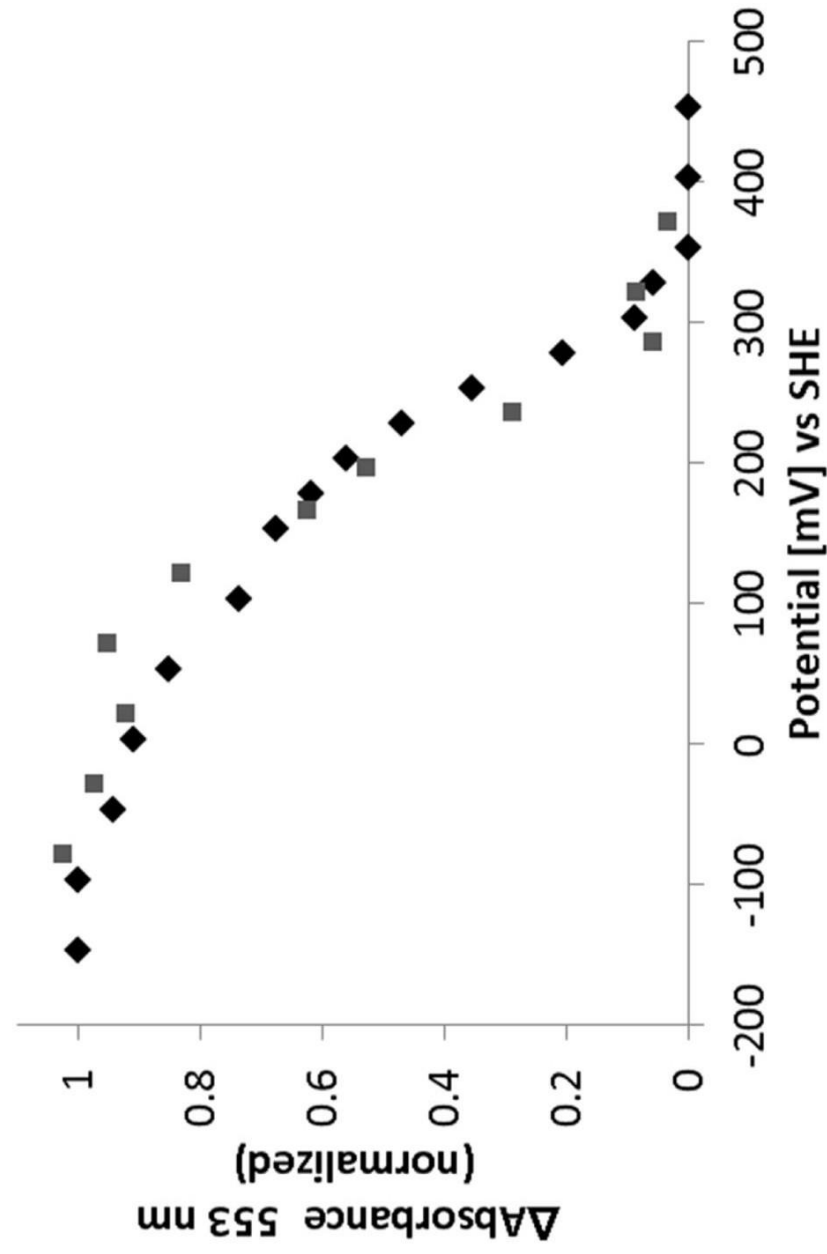


Figure 5

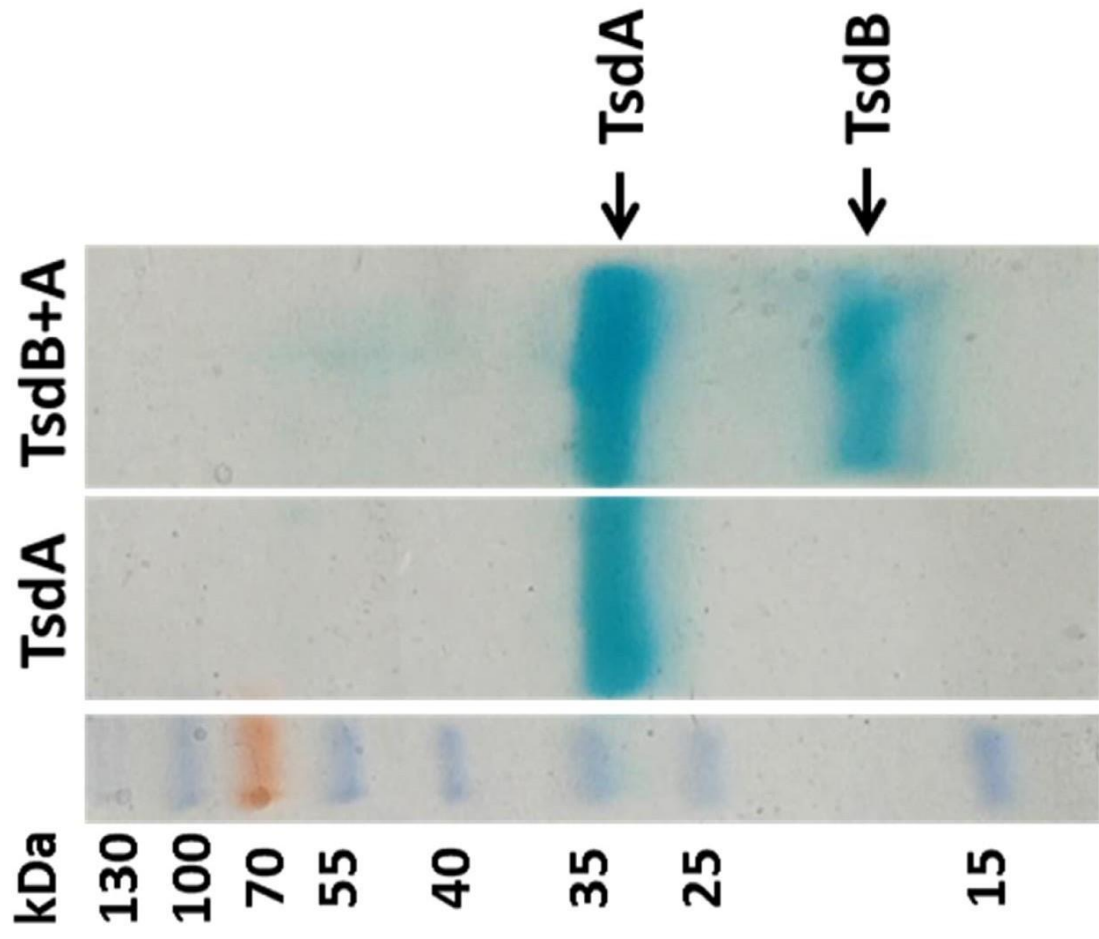


Figure 6

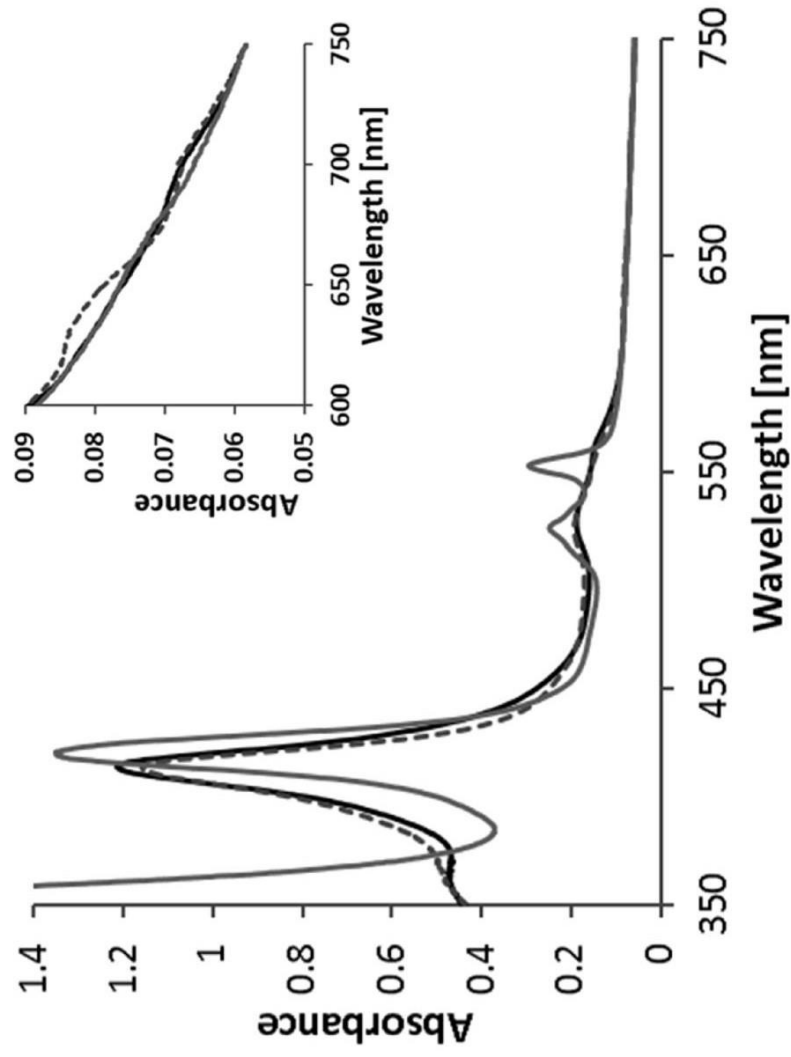


Figure 7

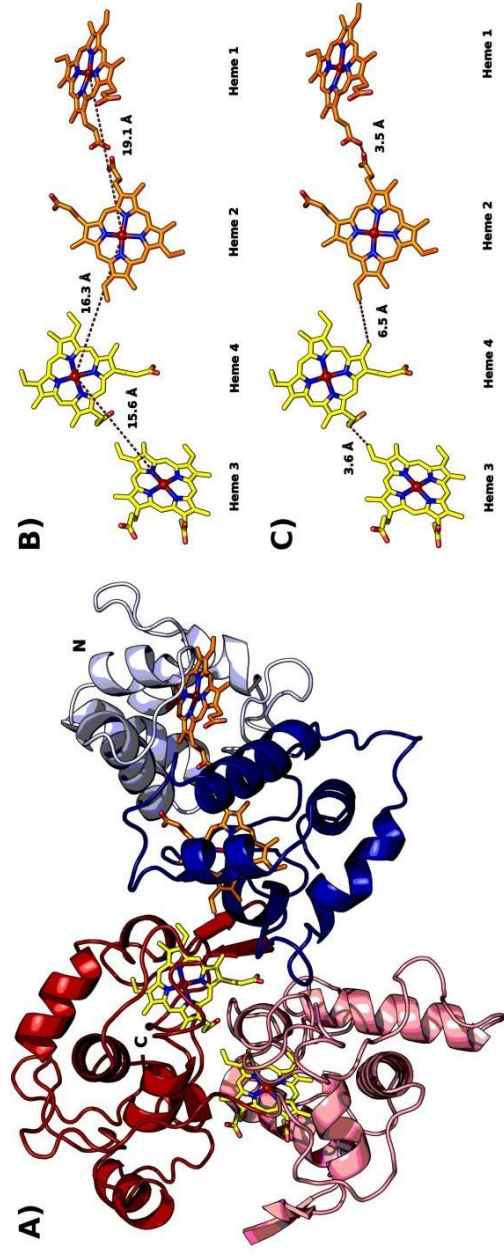


Figure 8

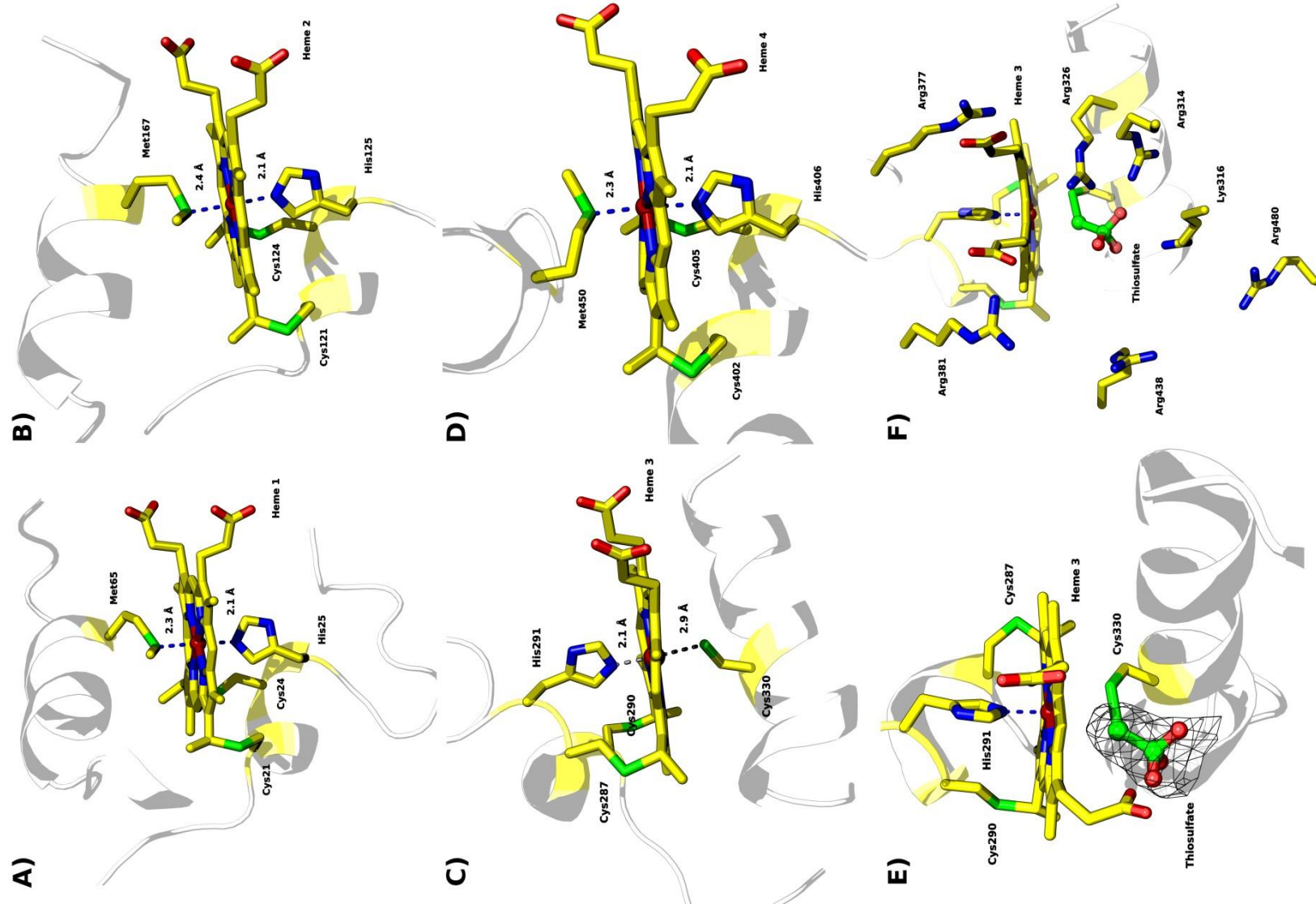


Figure 9

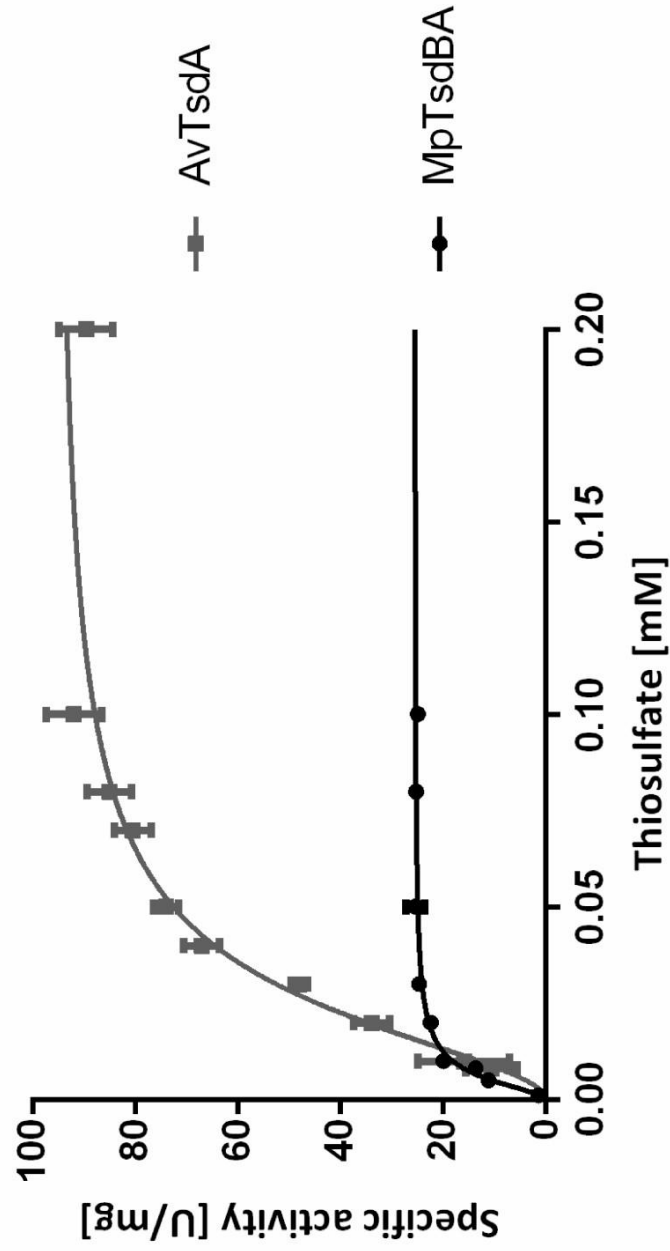


Figure 10

